Potential Solution to Strong CP violation: $X^{\pm}$ model

by

A thesis submitted to the School of Graduate Studies in partial fulfillment of the requirements for the degree of

M.Sc
Department of Physics and Physical Oceanography
Memorial University of Newfoundland

September 2016

St. John's Newfoundland

Abstract

The strong charge parity (CP) violation has been an open problem for many years. Expanding the current standard model (SM) to include new physics particles is a potential approach to explain it. To do so, $X^{\pm}$ was introduced with X^{+} coupling to anti-ferimion current and X^{-} to fermion current. As possible channels for searches for $X^{\pm}$, we have considered X^{+} in $e^{+}-e^{+}$ scattering and X^{-} in $e^{-}-e^{-}$ scattering. The difference between the cross sections was calculated using Mathematica with packages FeynArts, FeynCalc, Form and LoopTools at one loop level accuracy. The results were displayed in the form of exclusion plots. In the exclusion plots, the possible range of physical parameters of the new particles were tested, such as masses, couplings and phase factors.

Feynman rules, amplitude calculation and different renormalization methods at one loop level were also discussed to demonstrate the algorithmic potential for cross section calculation. In addition, new models for FeynArts and FormCalc were programmed to include the new particles.

However, in order to further test the new physics particles influence on strong CP violation, more research is needed. More specifically, one must test the hadronic interactions for $X^{\pm}$.

Acknowledgements

I want to thank my family for supporting me throughout my life especially while studying in Canada. As an international student studying in Canada, I do feel extremely lucky that I have chosen Memorial University of Newfoundland. The support from every faculty member and every dear friend here helped me overcome all obstacles.

I am grateful for this precious opportunity offered by my superiors Dr. Svetlana Barkanova and Dr. Aleksandrs Aleksejevs. I also want to thank Memorial University of Newfoundland and NSERC for funding my research. Special thanks to Kyle Marshall for his generous help with the revision.

Table of Contents

Chapter 1

Introduction

1.1 Introduction

According to cosmic microwave background (CMB) measurements, Big Bang nucleosynthesis calculates that net baryon number (n_B) to photon number (n_γ) ratio is significantly higher than the theoretical prediction, which assumes there was symmetrical distribution of baryons and anti-baryons at the beginning of the universe.

CMB calculation [32]:

$$\frac{n_B}{n_\gamma}_{\text{CMB}} = (6.14 \pm 0.25) \times 10^{-10};$$

Theoretical prediction [13]:

$$\frac{n_B}{n_\gamma}_{\text{theory}} = \frac{\bar{n}_B}{n_\gamma}_{\text{theory}} = 2 \times 10^{-18}$$

This disagreement in $\frac{n_B}{n_\gamma}$ directly leads to baryon and anti-baryon asymmetry, which is known as baryogenesis. In 1967, Andrei Sakharov proposed three conditions to explain baryongenesis [35]:

1. Baryon number violation;

2. C (charge conjugation) symmetry and CP (charge conjugation and parity)

symmetry violation;

3. Interactions out of thermal equilibrium;

which are the main motivation to study CP symmetry violation. Charge symmetry is already known to be broken in electromagnetic interaction, since the interaction depends on the sign of the charge. On the other hand, CP symmetry refers to particle-antiparticle symmetry, under the assumption of CPT invariant. In other words, if a particle and its antiparticle have different interactions, CP symmetry is violated. CP violation is an extremely rare phenomenon. However, it has been observed among standard model particles. But first, we need to look into the general concept of the standard model.

1.2 Standard Model

The standard model is a leading particle physics theory where all known matter and interactions (except gravity) can be described by elementary subatomic particles. Long before the major developments in science, an ancient Greek philosopher, Democritus, summed up some previous philosophic views of the world and proposed the idea of "atom" ($\alpha\tau\omega\mu\omega\sigma$ in Greek) – everything in the world is constructed by uncuttable "atoms" that either attract or repulse each other [33]. In 1897, J.J. Thomson discovered the electron. It was the first step to seek a further understanding of atoms. In the following century, many more subatomic particles were discovered and the corresponding theory was developed over time as well. And in 1978, the SM was proposed and still remains today, mostly accurate, but incomplete.

In the SM, all elementary particles fall into two classifications - fermions and bosons. Fermions are defined as particles with half integer spin (e.g. 1/2, 3/2). Bosons are defined as particles with integer spin. Different spins cause fermions and bosons behave and function differently. Fermions are associated with matter and bosons are

force carriers (Note Higgs bosons are not force carriers, which will be explained in the following "Bosons" section.) The SM still shares a similar concept with the ancient Greek scholar; however, there are a variety of "atoms" (Fermions) that couple to bosons.

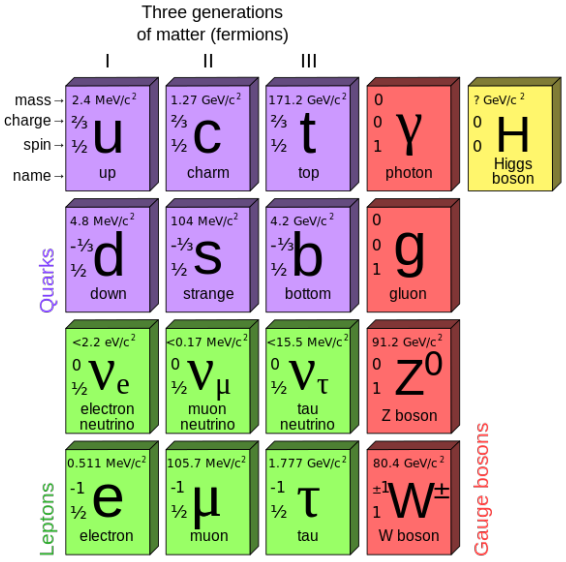

Figure 1.1: An instructive diagram for SM. (Credit: Holger Fiedler nach Benutzer: Murphee via Wikimedia Common, CC BY-SA [37].)

1.3 Fermions

Fermions obey the Pauli Exclusion Principle, which states no two identical and bound particles can occupy the same quantum state simultaneously. Two identical fermions, for example electrons, in an atom would not appear in the same orbit with the same spin. At least one of these two electrons need to be different to make the scenario physically possible. The Pauli Exclusion Principle is a distinctive feature for all fermions, which is identified by the physical property of half integer spins. In the SM, all elementary fermions can be further divided into quarks and leptons as shown in Fig.1.1 [21].

1.3.1 Quarks

The existence of quarks was independently proposed by Murray Gell-Mann and George Zweig in 1963 [18], and experimentally verified in 1968 at Stanford Linear Accelerator Center. The scattering distribution generated by emitting high energy electron beams into liquid hydrogen reveals that protons and neutrons consist of even smaller particles –quarks [33]. The original quark model only consists of 3 quarks (up, down and strange) which was used to explain the formation of new hadrons, where the strange (s) quark was introduced to explain unusual particles in the cosmic ray. Later the charm quark and bottom quark were discovered in the 1970s. And in 1995, the last piece of the quark section was completed with the detection of the top quark [2]. However, the top quark is unexpectedly massive – 186 times the mass of a proton. Due to the uncertainty principle, the massive top quarks have a much shorter time of existence, which prevents them from interacting with other quarks to form hadrons.

In total, there are 3 generations of quarks, up (u) and down (d), strange (s) and charm (c), top/truth (t) and bottom/beauty (b), which are classified by isospin.

$$\begin{pmatrix} u \\ t \\ c \end{pmatrix} \rightarrow T_3 \rightarrow \frac{1}{2}, \qquad \begin{pmatrix} d \\ s \\ b \end{pmatrix} \rightarrow T_3 \rightarrow -\frac{1}{2}$$

There is also a significant mass increase between higher generations and lower generations as shown in Fig. 1.1. Despite the difference in mass between generations, the interactions within each generation remains identical. Each type/flavour of quark also has 3 different color charges and a corresponding antiquark.

Quarks can interact by the strong interaction and form composite particles. Three bound quarks with -1/2 or -3/2 spin are called baryons, such as protons (uud), neutrons (udd) and their resonances. Two bound quarks can form mesons, which are spin 0 or

spin 1 particles, such as pions π and kaons K. Note the spin of mesons are integers, which indicates they are bosons.

1.3.2 Leptons

Unlike quarks, leptons cannot interact with each other via strong interaction. However, much like quarks, there are 6 flavours of leptons and they fall into 3 generations as well. Each generation of lepton includes a particle with a charge of e, electron for the first generation, muon for the 2nd generation, tau for the 3rd generation and their corresponding neutrino. The masses of leptons increase from lower generation to higher generation. The interactions within each lepton generation are identical as well.

There is a corresponding neutrino in each generation – a particle with very small mass and only interacts with matter through weak interaction. In fact, a single neutrino could travel through millions of kilometres of steel without being detected. The idea of the neutrino was proposed by Wolfgang Pauli in 1930 to explain some missing energy from nuclear β decay as an undetectable particle which transferred energy [7]. The 1st experimental observation of neutrino was done by Clyde Cowan and Fred Reines in 1956 [12]. The experiment was done using a nuclear reactor as the neutrino source and a large water tank as the "receiver". Gamma radiation was detected from the interactions between neutrinos and the atoms of water inside the tank.

For the other half of the generation, electrons, muons or taus share similar characteristics, because they have the same isospin and charge. Muons and taus can be considered as massive replicas of electrons. Due to the larger mass, muons and taus are highly unstable and tend to decay into less massive particles in less than a microsecond.

1.4 Bosons

Unlike fermions, bosons do not obey the Pauli Exclusion Principle. Bosons with the same energy can occupy same place in quantum space, which allows bosons to be interaction carriers.

Force	Strength	Range	Theory	Mediator
Strong	10	10^{-15} m	Chromodynamics	Gluon
Electromagnetic	10^{-2}	$1/r^2$	Electrodynamics	Photon
Weak	10^{-13}	10^{-18} m	Flavordynamics	W and Z
Gravitational	10^{-42}	$1/r^2$	Geometrodynamics	Graviton

Table 1.1: Summary of 4 fundamental forces and the corresponding boson mediators.

In the SM, all four fundamental forces are "carried" by four gauge bosons with corresponding dynamic theory, shown in Table 1.1 [18]. Unfortunately, the graviton still remains undetected and gravitational force has not yet been fully explained by SM. However, the strength scale of gravitational force is considerably smaller compared to the other fundamental forces. For this reason gravitational force will not be included in the following chapters. The Higgs boson is also an important part of SM, but not as a force carrier.

1.4.1 Gauge Bosons

Gauge bosons are introduced to quantize the four fundamental forces. The classic view of a field and corresponding interaction can be explained by exchange of corresponding gauge bosons.

Consider an electron which scatters with a muon and exchanges momentum and energy due to the electromagnetic force. In this scenario the corresponding gauge boson is the photon. In classical view, the electron and the muon change energy and momentum due to the coulomb force acting on them. On the other hand, it can also be explained by introducing the photon into the system. The electron loses/gains energy and momentum by emitting/absorbing a photon. The photon travels to, and is absorbed by, the muon which gains the exchanged energy and momentum. Similar process can happen due to different forces and the corresponding mediators. Of course, this example is extremely simplified. More complicated scattering process will be explained in detail in the future chapters.

In the classic view, interactions occur at a single point, which means there is no need for mediators. In fact, the "classic" Fermi model has accurate approximation results at low energies. However, in high energy conditions, the "classic" Fermi model fails and eventually is replaced by the intermediate vector boson theory.

1.4.2 Higgs Boson

As the last discovered piece of the SM, Higgs bosons play a vital role in the SM. Instead of a force carrier for fundamental forces, the Higgs boson is the "carrier" for the Higgs field, which is included in SM as a mass gaining field. The Higgs mechanism describes the spontaneous symmetry breaking in the Lagrangian of ground state. Only inside the Higgs field, all fundamental particles in the SM can obtain mass. Otherwise, the SM would not be functional [11]. Note that unlike force, mass is a scalar, which indicates its mediator Higgs bosons are supposed to be scalar bosons instead of vector bosons. The Higgs boson model was proposed independently by three groups (Guralnik, Hagen and Kibble; Higgs; Brout and Englert) [11]. It was finally discovered

experimentally at CERN in June, 2012, filling in this important piece of the SM [34].

1.5 SM Symmetry

Mathematically, quantum field theory is the foundation of the standard model. Quantum field theory is using the Lagrangian of fields to provide the theoretical structure of the interactions. In the SM, there are three symmetry groups: SU(3), SU(2) and U(1). Each symmetry group is associated with corresponding fields. U(1) consists of hyper charge, SU(2) consists of 3 isospin fields and SU(3) symmetry is called the colour/flavor group, as shown in Figure 1.2.

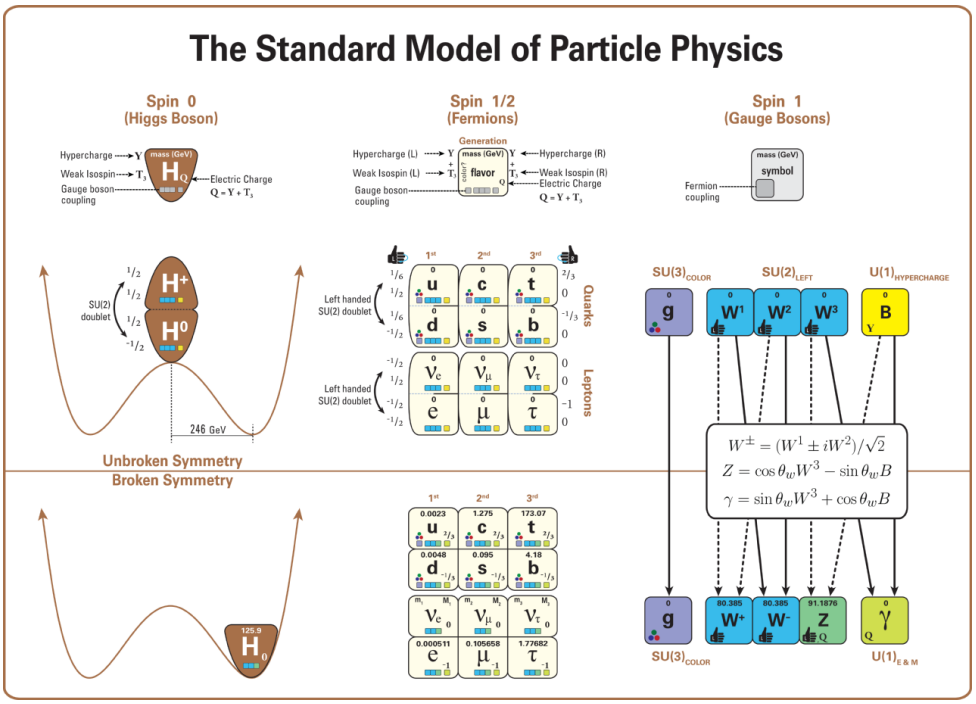

Figure 1.2: Symmetry groups for SM [38].

Note that both weak isospin fields and hyper charge are not involved in the SM directly, which involves the Higgs fields and spontaneous symmetry breaking. Isospin fields (W^1, W^2, W^3) and hyper charge interact and form $W^{\pm}$, Z bosons and photon in the way shown in Figure 1.2. However, neither the isospin fields, hyper charge or the

newly formed bosons have mass. After interacting with the Higgs fields, known as spontaneous symmetry breaking, those gauge bosons obtain mass. The interesting hat shape Higgs-field Lagrangian provides a non-zero ground state, which means non-zero mass.

Although the detail of the spontaneous symmetry breaking does not have an impact on the calculations for this research, the hyper charge and weak isospin fields are involved in many derivations of these calculations beyond the quantum electrodynamics (QED) level.

1.6 CP Violation in SM

1.6.1 CP Violation in the Quark Sector

As mentioned earlier this chapter, there are observed occurrences of CP violation within the SM. In 1964, Cronin and Fitch discovered CP violation in neutral kaon K^0 decays in to two charged pions ($\pi^{\pm}$) [10].

$$K_L^0 \rightarrow \pi^+ + e^- + \bar{\nu}_e$$

$$K_L^0 \rightarrow \pi^- + e^+ + \nu_e$$

Note here that L in K_L^0 only refers to the parity of the kaon. If CP was invariant, these two process would be identical. The experimental result proves that the positron decay mode happens more often than the electron mode.

In order to include the CP violation into the SM, the Cabibbo–Kobayashi–Maskawa

matrix (CKM matrix) was introduced as a parameterization [9].

$$V = \begin{pmatrix} V_{ud} & V_{us} & V_{ub} \\ V_{cd} & V_{cs} & V_{cb} \\ V_{td} & V_{ts} & V_{tb} \end{pmatrix} = \begin{pmatrix} c_1 & -s_1c_3 & -s_1s_3 \\ s_1c_2 & c_1c_2c_3 - s_2s_3e^{i\delta} & c_1c_2s_3 + s_2c_3e^{i\delta} \\ s_1s_2 & c_1s_2c_3 + c_2s_3e^{i\delta} & c_1s_2c_3 - c_2c_3e^{i\delta} \end{pmatrix}$$

Different flavoures can be mixed through the CKM matrix, and the process is in the form of

$$\begin{pmatrix} d' \\ s' \\ b' \end{pmatrix} = \begin{pmatrix} V_{ud} & V_{us} & V_{ub} \\ V_{cd} & V_{cs} & V_{cb} \\ V_{td} & V_{ts} & V_{tb} \end{pmatrix} \begin{pmatrix} d \\ s \\ b \end{pmatrix}.$$

The mixing process is a unitary transformation, which means

$$\sum_k |V_{ik}|^2 = \sum_i |V_{ik}|^2 = 1$$

Here the CP violation is parameterized in the complexed phase $e^{i\delta}$. As long as δ does not equal 0, CP violation exists in the quark sector. The entire CKM matrix has been successfully measured in experiments and the contribution of the CP violating phase has proven to be the order of 10^{-3} which is not sufficient for baryongenesis [8]. Therefore, it is known as the weak CP violation in contrary to the strong CP violation. Despite the small magnitude, the discovery of CP violation in the quark sector inspired many people to search for other possibilities.

1.6.2 CP Violation in the Lepton Sector

The discovery of neutrino oscillation reveals the physics behind lepton mixing. Similar to the CKM matrix, the Pontecorvo–Maki–Nakagawa–Sakata matrix (PMNS

matrix) was proposed as the mixing matrix [28].

$$\begin{pmatrix} \nu_e \\ \nu_\mu \\ \nu_\tau \end{pmatrix} = \begin{pmatrix} U_{e1} & U_{e2} & U_{e3} \\ U_{\mu 1} & U_{\mu 2} & U_{\mu 3} \\ U_{\tau 1} & U_{\tau 2} & U_{\tau 3} \end{pmatrix} \begin{pmatrix} \nu_1 \\ \nu_2 \\ \nu_3 \end{pmatrix}.$$

Here $\nu_{1,2,3}$ are the mass eigenstates of neutrinos and $\nu_{e,\mu,\tau}$ are the energy eigenstates of neutrinos. Each one of the mass eigenstate of neutrinos are a combination of all the energy eigenstates and the combination pattern oscillates. Similarly, the CP violation is parameterized in the PMNS matrix as well [22].

$$\begin{pmatrix} U_{e1} & U_{e2} & U_{e3} \\ U_{\mu 1} & U_{\mu 2} & U_{\mu 3} \\ U_{\tau 1} & U_{\tau 2} & U_{\tau 3} \end{pmatrix} = \begin{pmatrix} c_{12}c_{13}e^{i\delta_{13}} & s_{12}c_{13}e^{i\delta_{13}} & s_{13} \\ -s_{12}c_{23} - c_{12}s_{23}s_{13}e^{i\delta_{13}} & c_{12}c_{23} - s_{12}s_{23}s_{13}e^{i\delta_{13}} & s_{23}c_{13} \\ s_{12}s_{23} - c_{12}s_{23}s_{13}e^{i\delta_{13}} & -c_{12}s_{23} - s_{12}c_{23}s_{13}e^{i\delta_{13}} & c_{23}c_{13} \end{pmatrix}$$

The direct measurement of the CP violating phase $e^{i\delta_{13}}$ is still a work in progress. Due to the nature of neutrinos, their detection is extremely difficult. With the combined effort of SNOlab and the Super-Kamiokande experiment, people have already found that the neutrino mass exists and it is the key solution to neutrino oscillation. For this reason, the Nobel Prize in Physics 2015 was awarded jointly to Takaaki Kajita and Arthur B. McDonald. The CP violation in the lepton sector is the most promising candidate for strong CP violation, because the baryongenesis can be achieved from leptogenesis [26].

The small mass scale of neutrinos raises the question that if neutrinos are Majorana fermions, unlike Dirac fermions, then they do not obtain their mass term from Higgs mechanism. Instead, the Majorana mass term comes from the Majorana equation where a Majorana fermion is its own antiparticle during propagation [30]. If neutrinos are

proven to be Majorana, it opens more theoretical potential for CP violation detection in the lepton sector.

1.7 CP Violation Beyond Standard Model

There are many observations that cannot be explained by the current version of the SM, such as gravity, the hierarchy problem, the absolute mass of neutrinos, dark matter and strong CP violation. These limitations of the SM lead people to believe that there are new physics particles yet to be discovered. The theoretical calculations with new physics particle models could provide important information, such as potential mass and precision requirements, for their discovery.

With the assumption that neutrinos are Majorana fermions, the seesaw mechanism provides a solution to strong CP violation beyond standard model (BSM) [3]. The seesaw mechanism introduces heavy seesaw neutrinos as partners of SM neutrinos. The seesaw relationship suggests that seesaw neutrinos are extremely massive in the opposite fashion that SM neutrinos are extremely light. They are CP violating big bang particles which formed the early universe and resulted in the baryongenesis and other phenomena in CMB, such as dark matter in the early universe [27]. It is one of the most popular theories for strong CP violation.

The extreme mass scale of seesaw neutrino is at 10^{10} to 10^{16} GeV [25], which is impossible to be produced at the Large Hadron Collider (LHC) in the near future. Therefore, experiments on the seesaw mechanism only focus on the SM part. Double beta decay is the key experiment to examine the CP violation and Majorana mass of SM neutrinos. *Neutrinoless Double Beta Decay Experiments* by Alberto Garfagnini is a general review of current double beta decay experiments [17].

Another popular topic for strong CP violation BSM is the Supersymmetry model (SUSY). There are many versions of SUSY, but in general, SUSY is an expansion of current SM. It suggests that there is a superpartner for every SM particle. For a fermion,

its superpartner is a boson and for a boson, its superpartner is a fermion. SUSY can provide strong CP violation with flavour violation [4][24][23]. The main problem for the SUSY model is that with the recent development at the LHC, there is still no discovery for any SUSY superpartners. Unlike seesaw neutrinos, there is no specific reason why SUSY superpartners should be extremely light or massive compared to SM.

1.8 $X^{\pm}$ Model

The $X^{\pm}$ model uses a set of similar conduits as the $W^{\pm}$ prime model-charged currents with new physics particles. However, the $W^{\pm}$ prime model is designed to study the spins/helicity of fermions, not the strong CP violation [1]. Instead of using neutrino oscillations or superpartners as the focus to study the strong CP violation, the $X^{\pm}$ model assigns a direct CP violating phase through BSM vector boson X^{+} and X^{-}. This model links SM particles and the dark $D^{\pm}$ particles through a new physics particles (NP) loop. The $D^{\pm}$ particles and NP loop are introduced as the physical origin of the $X^{\pm}$ particles. However, one can only observe them as the $X^{\pm}$ particle altogether. The advantage of this model is that the coupling between the dark particles and the Standard Model particle is hidden away from direct interaction.

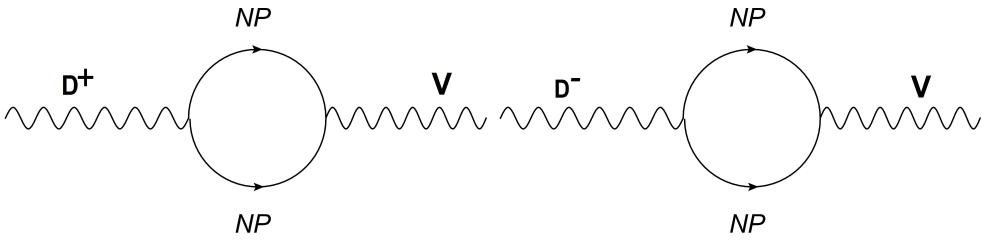

Figure 1.3: $D^{\pm}$ interacts with SM through a new physics particles (NP) loop.

Recall in the CKM matrix and PMNS matrix, the CP violation parameterization uses a complex phase in the form of $e^{i\delta}$. The entries in both matrices with such phase almost always consists of a nonzero real term in addition to the complex phase term. The combination between the real and complex terms is why one can express the CP

violation in such a manner. $|V_{ik}|^2$ or $|U_{ik}|^2$ differs from $|V_{ik}^*|^2$ or $|U_{ik}^*|^2$; therefore, it is essential for X^+ and X^- to each consist of two Feynman diagrams with different type of phases.

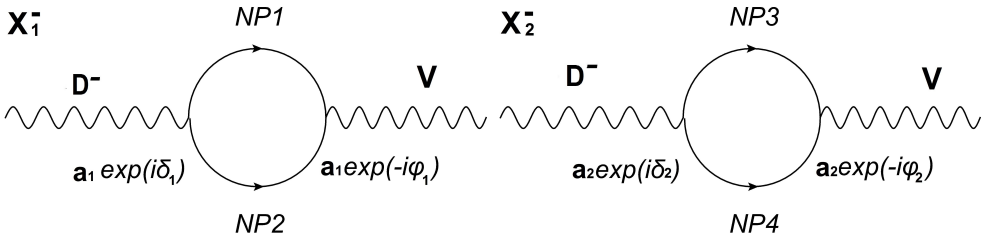

Figure 1.4: The two component Feynmen diagrams for the X^- model.

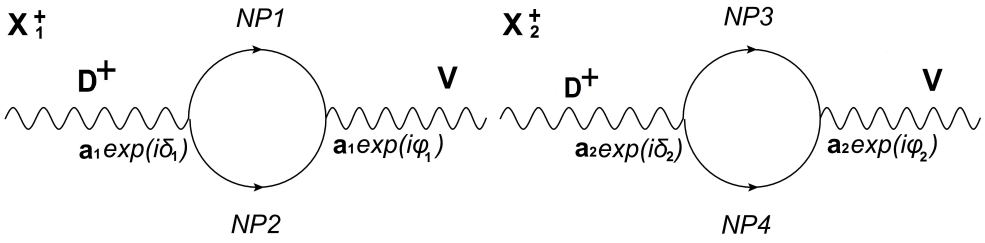

Figure 1.5: The two component Feynmen diagrams for the X^+ model.

The phases were parameterized by me into $X^\pm$ coupling:

$$X^+ : \mu_1 = a_1^2 e^{i\delta_1 + i\phi_1} + a_2^2 e^{i\delta_2 + i\phi_2}, \tag{1.1}$$

$$X^- : \mu_2 = a_1^2 e^{i\delta_1 - i\phi_1} + a_2^2 e^{i\delta_2 - i\phi_2}, \tag{1.2}$$

where a_1 and a_2 are the coupling constants for vertices of each component of the $X^\pm$ respectively. At each vertex there is a phase factor assigned. The right vertex contains the electro-weak phase, and the other vertex contains the strong phase. The electro-weak phase is related to the electro-weak interaction between SM particles and the new physics particles loop, while the strong phase is related to the strong interaction between the $D^\pm$ and the new physics particles loop. Based on the different interactions, the phases become different for the new physics particles loop. For electro-weak interactions,

the CP operation changes the phase of the coupling. On the other hand, for strong interactions, the CP operation does not influence the phase. As a result, the difference between the X^+ and X^- in coupling directly produces the strong CP violation.

1.9 Summary

The strong CP violation is the key to explain baryongenesis. With the discovery of weak CP violation in the CKM matrix and ongoing measurement of the complete PMNS matrix, the progress to solve such a problem is promising. However, due to the nature of neutrinos, neutrino physics experiments are often extremely challenging. Dr. Aleksejevs and I proposed the $X^{\pm}$ model, a potential neutrinoless solution to the strong CP violation. Unlike SUSY, the $X^{\pm}$ model does not have superpartner properties and only serves as a medium to implant CP violating phases.

Chapter 2

Cross Section and Feynman Rules

In order to test $X^{\pm}$ theoretically, one needs to calculate a physical measureable involving $X^{\pm}$ particles. Thanks to the $X^{\pm}$ model, the new particles, $X^{\pm}$, are similar to $W^{\pm}$ mathematically. The main differences are the $X^{\pm}$ have an additional CP violating phase, X^{+} does not couple with e^{-} and X^{-} does not couple with e^{+}. Therefore, the $X^{\pm}$ model has a great advantage to inherit most of the calculation techniques and renormalization schemes from the SM with minimum modification.

2.1 Cross Sections and Fermi's Golden Rule

The scatter distribution is the physical observable for particle collision experiments. In other words, the possibility of finding scattered particles at certain locations can be measured. The cross section (σ) is introduced to represent such possibility. Consider an incoming beam of particles that scatters with stationary particles. The overall cross section area of all the scattered particles is σ_{tot}. After the scattering, n particles are deflected into different directions and at a certain direction there will be particles with effective cross section area of σ_i, and a total cross section of

$$\sigma_{tot} = \sum_{i=1}^{n} \sigma_i,$$

the ratio of σ_i to σ_{tot} corresponds to the possibility of finding particles at a certain direction [11].

Fermi's Golden Rule connects between the experimental cross section and the theoretical wave function. If 1 and 2 are incoming particles and particles 3 and 4 are the products of the scattering,

$$1 + 2 \ \rightarrow \ 3 + 4, \tag{2.1}$$

Fermi's golden rule is

$$\begin{aligned}\sigma =& \frac{S\hbar^2}{4\sqrt{(p_1 \cdot p_2)^2 - (m_1 m_2)^2}} \int |\mathscr{M}|^2 (2\pi)^4 \delta^4(p_1 + p_2 - p_3 - p_4) \\ & \times \prod_{j=3}^{4} 2\pi\delta(p_j^2 - m_j^2)\theta(p_j^0)\frac{d^4 p_j}{(2\pi)^4},\end{aligned} \tag{2.2}$$

where $\mathscr{M}$ is the amplitude, θ is the Heaviside step function, p_j and m_j (j=1,2,3,4) are the 4-momentum and mass for the i particle, δ is the Delta function and S is the symmetry factor. If particles 3 and 4 are identical, S will be $2! = 2$ and if they are not identical, S will be 1. There are 3 features in this equation:

1. The Delta function $\delta^4(p_1 + p_2 - p_3 - p_4)$ guarantees energy-momentum is conserved;

2. The Delta function $\delta(p_j^2 - m_j^2)$ ensures the product particles (particles 3 and 4) have to be on shell (physically observable);

3. The Heaviside step function $\theta(x) = \begin{cases} 0 & \text{if } x < 0 \\ 1 & \text{if } x > 0 \end{cases}$ constrains the energy of each product particle to be positive.

Fermi's golden rule mainly depends on kinematic conditions of the particles, except the amplitude $\mathscr{M}$, which is associated with the Lagrangian of interacting fields and contains the dynamics of the scattering [31], which can be obtained through Feynman

rules.

2.2 Feynman Rules

The amplitude of the scattering $\mathscr{M}$ needs to be calculated. It is directly involved in the calculation of cross sections. As previously stated, the amplitude is closely related to the Lagrangian of interacting fields. It can be solved from the Lagrangian expression directly. However, American physicist Richard Feynman developed Feynman Calculus (including the Feynman diagram) to calculate the amplitude in an effective and algorithmic way.

Feynman diagrams are not only a general graphic demonstration of the topology of scattering process, but also contains the mathematical information to construct the amplitude calculation. Thanks to Feynman rules, one can construct amplitude by assembling different terms according to the structure of the corresponding Feynman diagram.

All the descriptions of Feynman rules can be found on *Introduction to Elementary Particles* by David Griffiths [18].

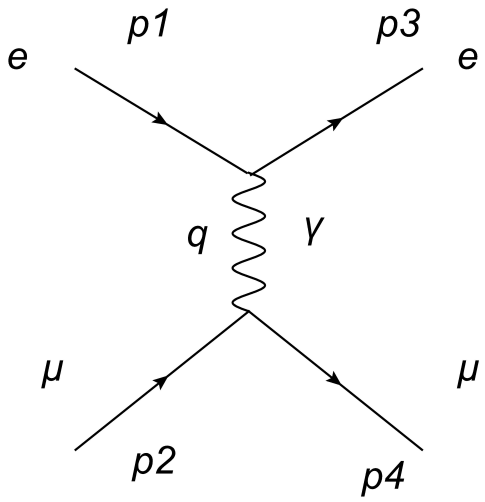

Figure 2.1: Feynman diagram for electron-muon scattering.

Using the electron-muon scattering as an example, the Feynman diagram is shown in Fig. 2.1. The external particles are the incoming electron (p_1, s_1) and muon (p_2, s_2) and the outgoing electron (p_3, s_3) and muon (p_4, s_4). The internal particle is the photon. There are two vertices in the diagram. One is connecting to the two electrons and the photon and the other is connecting to the two muons and the photon. According to the Feynman rules, the following terms should be written down:

1. Four external lines: Dirac spinors $u_e(p_1, s_1),\ \bar{u}_e(p_3, s_3),\ u_{muon}(p_2, s_2),\ \bar{u}_{muon}(p_4, s_4)$;
2. Two (same) vertices coupling: $ig_e\gamma^\mu$ and $ig_e\gamma^\nu$;
3. The propagator: $\frac{-ig_{\mu\nu}}{q^2}$;
4. Two delta functions and integration term: $\delta^4(p_1 - p_3 - q)\delta^4(p_2 - p_4 + q)\frac{d^4q}{(2\pi)^4}$.

At the moment, the expression is

$$\begin{aligned}\mathscr{M} =&(2\pi)^4 \int [\bar{u}_e(p_3, s_3) ig_e\gamma^\mu u_e(p_1, s_1)] \frac{-ig_{\mu\nu}}{q^2} [\bar{u}_{muon}(p_4, s_4) ig_e\gamma^\nu u_{muon}(p_2, s_2)] \\ &\times \delta^4(p_1 - p_3 - q)\delta^4(p_2 - p_4 + q) d^4q\end{aligned} \tag{2.3}$$

After solving the delta functions, the amplitude $\mathscr{M}$ becomes

$$\mathscr{M} = \frac{-ig_e}{(p_1 - p_3)^2}[\bar{u}_e(p_3, s_3)ig_e\gamma^\mu u_e(p_1, s_1)][\bar{u}_{muon}(p_4, s_4)ig_e\gamma_\mu u_{muon}(p_2, s_2)] \tag{2.4}$$

If the kinematic information (p_i and s_i, $i = 1, 2, 3, 4$) is provided, then the amplitude $\mathscr{M}$ can be calculated numerically.

2.2.1 Feynman Rules for $X^\pm$

Feynman rules were derived from QED field Lagrangian using functional derivative of the path integral [16]. The field Lagrangian density $\mathscr{L}$ consists of 3 terms-the kinematic term ($\mathscr{L}_{KE}$), the mass term ($\mathscr{L}_M$) and the interaction term ($\mathscr{L}_{Int}$).

$$\mathscr{L} = \mathscr{L}_{KE} + \mathscr{L}_M + \mathscr{L}_{Int}$$

Using the functional derivative of the path integral on $\mathscr{L}_{Int}$, one can obtain the coupling for the Feynman rules

$$S_1 = \frac{\delta^n}{\delta V_1(k_1)\delta V_2(k_2)\delta V_3(k_3)\cdots\delta V_n(k_n)} \int d^4x \mathscr{L}_{Int}. \tag{2.5}$$

$$\Gamma = iS_1 \tag{2.6}$$

Using the functional derivative of path integral on $\mathscr{L}_{KE} + \mathscr{L}_M$, one can obtain the propagator for the Feynman rules

$$S_2 = \frac{\delta^n}{\delta V_1(k_1)\delta V_2(k_2)\delta V_3(k_3)\cdots\delta V_n(k_n)} \int d^4x (\mathscr{L}_{KE} + \mathscr{L}_M) \tag{2.7}$$

$$i\Pi = iS_2^{-1} \tag{2.8}$$

In this research, Dr. Aleksejevs and I propose the Lagrangian density of $X^\pm$ or X field interacting with a fermion field and an anti-fermion field are calculate the corresponding

Feynman rules. The interaction Lagrangian of the $X^{\pm}$ interacting with fermions is

$$\mathscr{L}_{int} = \frac{1}{12} g_1 \bar{u}_1 \gamma^\mu \omega_- u_2 X^-_\mu + \frac{1}{12} g_2 \bar{v}_2 \gamma^\mu \omega_+ v_1 X^+_\mu, \tag{2.9}$$

where

$$\omega_\pm = \frac{1 \pm \gamma_5}{2},$$

$$g_1 = \frac{e}{\sin\theta_W}\left(a_1^2 e^{i\delta_1 + i\phi_1} + a_2^2 e^{i\delta_2 + i\phi_2}\right),$$

$$g_2 = \frac{e}{\sin\theta_W}\left(a_1^2 e^{i\delta_1 - i\phi_1} + a_2^2 e^{i\delta_2 - i\phi_2}\right),$$

and θ_W is the weak mixing angle.

$\mathscr{L}_{int}$ consists of two parts. One is the fermion field (u_2), the anti fermion field $\bar{u_1}$ and vector boson field X^-. The other one is the CP conjugation of the first half, with v_1, $\bar{v}_2$ and X^+. $u_{1,2}$ and $v_{1,2}$ are the solutions to the Dirac equations and $X^{\pm}$ are the solutions for Klein Gordon equation for plane wave functions. Therefore, I apply the functional derivative method from Eqn. 2.5 to one half of the $\mathscr{L}$ at a time.

$$\begin{aligned}
S_{1,X^-} =& \frac{1}{12}\frac{\delta^3}{\delta u_1(k_1)\delta u_2(k_2)\delta X(k_3)} \int d^4x \;\; g_1 \bar{u}_1(x_1)\gamma^\mu \omega_- u_2(x_2) X^-_\mu(x_3) \\
=& \frac{1}{12}\frac{\delta^3}{\delta u_1(k_1)\delta u_2(k_2)\delta X(k_3)} \int d^4x d^4p_1 d^4p_2 d^4p_3 \;\; e^{-i(p_1+p_2+p_3)} g_1 \bar{u}_1(p_1)\gamma^\mu \omega_- u_2(p_2) X^-_\mu(p_3) \\
=& \frac{1}{12}\frac{\delta^2}{\delta u_1(k_1)\delta u_2(k_2)\delta} \int d^4x d^4p_1 d^4p_2 d^4p_3 \;\; e^{-i(p_1+p_2+p_3)} [g_1 \bar{u}_1(p_1)\gamma^\mu \omega_- u_2(p_2)\delta(k_3-p_3) + \\
& g_1 \bar{u}_1(p_2)\gamma^\mu \omega_- u_2(p_1)\delta(k_3-p_3) + g_1 \bar{u}_1(p_2)\gamma^\mu \omega_- u_2(p_3)\delta(k_3-p_1) + \\
& g_1 \bar{u}_1(p_3)\gamma^\mu \omega_- u_2(p_2))\delta(k_3-p_1) g_1 \bar{u}_1(p_1)\gamma^\mu \omega_- u_2(p_3)\delta(k_3-p_2) + \\
& g_1 \bar{u}_1(p_3)\gamma^\mu \omega_- u_2(p_1))\delta(k_3-p_2)] \\
=& \frac{1}{12} g_1 \gamma^\nu \omega_- \int d^4x d^4p_1 d^4p_2 d^4p_3 \;\; e^{-i(p_1+p_2+p_3)} \sum_{a\neq b\neq c\neq a}^{3} 2\delta(k_a-p_1)\delta(k_b-p_2)\delta(k_c-p_3) \\
=& \frac{1}{12} g_1 \gamma^\nu \omega_- \int d^4x d^4p_1 d^4p_2 d^4p_3 \;\; e^{-i(p_1+p_2+p_3)} \times 12 \\
=& g_1 \gamma^\nu \omega_- \delta(p_1+p_2+p_3).
\end{aligned} \tag{2.10}$$

The first step is using a Fourier transformation to move the base of the integral to the momentum space. Using the same procedures, I can also calculate

$$S_{1,X^+} = g_2\gamma^\nu\omega_+\delta(p_1+p_2+p_3). \tag{2.11}$$

Overall, the coupling portion of the Feynman rules is

$$\Gamma = iS_1 = i(S_{1,X^-} + S_{1,X^+} = i(g_1\gamma^\nu\omega_- + g_2\gamma^\nu\omega_+)\delta(p_1+p_2+p_3) \tag{2.12}$$

On the other hand, the calculation of the propagator is more complicated. The Lagrangian density for the kinematic term is

$$\mathscr{L}_{KE} = -\frac{1}{4}F^X_{\mu\nu}F_X^{\mu\nu} - \frac{1}{2\lambda}\partial_\mu X^\mu\partial_\nu X^\nu, \tag{2.13}$$

where

$$F^X_{\mu\nu} = \partial_\mu X_\nu - \partial_\nu X_\mu,$$

and λ is an arbitrary parameter for the gauge fixing term

$$-\frac{1}{2\lambda}\partial_\mu X^\mu\partial_\nu X^\nu.$$

The mass term is

$$\mathscr{L}_M = \frac{1}{2}m_X^2 X_\mu X^\mu. \tag{2.14}$$

Apply $\mathscr{L}_{KE}$ and $\mathscr{L}_M$ to Eqn. 2.7:

$$S_2 = \frac{\delta^2}{\delta X(k_1)\delta X(k_2)}\int d^4x d^4q_1 d^4q_2 \;\; e^{-i(q_1+q_2)}[\mathscr{L}_{KE}(x) + \mathscr{L}_M(x)]. \tag{2.15}$$

The integral part of S_2 is in the form of:

$$\begin{aligned}
&\int d^4x d^4q_1 d^4q_2 \;\; e^{-i(q_1+q_2)}[\mathscr{L}_{KE}(x)+\mathscr{L}_M(x)] \\
=&\int d^4x d^4q_1 d^4q_2 \;\; e^{-i(q_1+q_2)}\left\{-\frac{1}{4}\left[-iq_{1\mu}X_\nu(q_1)+iq_{1\nu}X_\mu(q_1)\right]\left[-iq_2^\mu X^\nu(q_2))+iq_2^\nu X^\mu(q_2)\right]\right. \\
&\left.+\frac{1}{2}m_X^2X_\mu(q_1)X^\mu(q_2)+\frac{1}{2\lambda}q_{1\mu}q_{2\nu}X^\mu(q_1)X^\nu(q_2)\right\}.
\end{aligned} \tag{2.16}$$

I apply the functional derivative method to this integral, with the field index α and β:

$$\begin{aligned}
S_2 =&\frac{\delta^2}{\delta X_\alpha(k_1)\delta X_\beta(k_2)}\int d^4x d^4q_1 d^4q_2 \;\; e^{-i(q_1+q_2)}[\mathscr{L}_{KE}(x)+\mathscr{L}_M(x)] \\
=&\frac{\delta}{\delta X_\alpha(k_1)}\int d^4x d^4q_1 d^4q_2 \;\; e^{-i(q_1+q_2)}\left\{-\frac{1}{4}[(-iq_{1\mu}g_{\beta\nu}\delta(k_2-q_1)\right. \\
&+iq_{1\nu}g_{\beta\mu}\delta(k_2-q_1))(-iq_2^\mu X_\nu(q_2)+iq_2^\mu X^\mu(q_2)) \\
&+(-iq_{1\nu}X_\nu(q_1)+iq_{1\nu}X_\mu(q_1))(-iq_2^\mu g_\beta^\nu\delta(k_2-q_2)+iq_2^\nu g_\beta^\nu\delta(k_2-q_2)) \\
&+\frac{1}{2}m_X^2(g_{\beta\mu}\delta(k_2-q_1)X^\mu(q_2)+g_\beta^\mu\delta(k_2-q_2)X_\mu(q_1))] \\
&\left.+\frac{1}{2\lambda}q_{1\mu}q_{2\nu}(g_\beta^\mu\delta(k_2-q_1)X^\nu(q_2)+g_\beta^\nu\delta(k_2-q_2)X^\mu(q_1))\right\} \\
=&\int d^4x d^4q_1 d^4q_2 \;\; e^{-i(q_1+q_2)}\cdot-\frac{1}{4}[(-iq_{1\mu}g_{\beta\nu}+iq_{1\nu}g_{\beta\nu})(-iq_2^\mu g_\alpha^\nu+iq_2^\nu g_\alpha^\nu)\delta(k_1-q_2)\delta(k_2-q_1) \\
&+(-iq_{1\mu}g_{\alpha\nu}+iq_{1\nu}g_{\alpha\mu})(-iq_2^\mu g_\beta^\nu+iq_2^\nu g_\beta^\mu)\delta(k_2-q_2)\delta(k_2-q_2)] \\
&+\frac{1}{2}m_X^2(g_{\beta\nu}g_\alpha^\mu\delta(k_2-q_1)\delta(q_2-k_1)+g_\beta^\mu g_{\alpha\mu}\delta(k_2-q_2)\delta(k_1-q_1) \\
&+\frac{1}{2\lambda}q_{1\mu}q_{2\nu}(g_\beta^\mu g_\alpha^\nu\delta(k_2-q_1)\delta(k_1-q_2)+g_\beta^\nu g_\alpha^\mu\delta(k_2-q_2)\delta(k_1-q_1).
\end{aligned} \tag{2.17}$$

The kinematic condition of the propagation is

$$k_{1\mu}=-k_{2\mu}=k_\mu,$$

which can simplify S_2:

$$\begin{aligned} S_2 = \int d^4x d^4q_1 d^4q_2 \;\; e^{-i(q_1+q_2)} \cdot -\frac{1}{4}[(ik_\mu g_{\beta\nu} - ik_\nu g_{\beta\nu})(-ik^\nu g^\nu_\alpha + ik^\nu g^\nu_\alpha) \\ + (-ik_\mu g_{\alpha\nu} + ik_\nu g_{\alpha\mu})(ik^\mu g^\nu_\beta - ik^\nu g^\mu_\beta)] \\ + \frac{1}{2}m_X^2(g_{\beta\nu}g^\mu_\alpha + g^\mu_\beta g_{\alpha\mu}) + \frac{1}{2\lambda}(-g^\nu_\beta g^\nu_\alpha k_\mu k_\nu - g^\nu_\beta g^\mu_\alpha k_\mu k_\nu). \end{aligned} \tag{2.18}$$

After the contraction of indices, I obtain the inverted propagator

$$\begin{aligned} S_2 = \mathscr{D}_{\alpha\beta} &= -k^2 g_{\alpha\beta} + k_\alpha k_\beta + m_X^2 g_{\alpha\beta} - \frac{1}{\lambda}k_\alpha k_\beta \\ &= -\left[(k^2 - m_X^2)g_{\alpha\beta} - \left(1 - \frac{1}{\lambda}\right)k_\alpha k_\beta\right]. \end{aligned} \tag{2.19}$$

In order to invert the inverted propagator, I use the identity

$$\mathscr{D}_{\alpha\beta}\Pi^{\alpha\rho} \equiv g^\rho_\beta,$$

whose solution has the form of

$$i\Pi^{\alpha\rho} = i\xi_1 g^{\alpha\rho} + i\xi_2 k^\alpha k^\rho.$$

Therefore, the final step to calculate $\Pi^{\alpha\rho}$ is to solve ξ_1 and ξ_2 from

$$\begin{aligned} \mathscr{D}_{\alpha\beta}\Pi^{\alpha\rho} &\equiv g^\rho_\beta \\ &= -[(k^2 - m_X^2)g_{\alpha\beta} - \left(1 - \frac{1}{\lambda}\right)k_\alpha k_\beta](\xi_1 g^{\alpha\rho} + \xi_2 k^\alpha k^\rho). \end{aligned} \tag{2.20}$$

The solution is

$$\xi_1 = -\frac{1}{k^2 - m_X^2},$$

and

$$\xi_2 = \frac{1-\lambda}{(k^2 - m_X^2)(k^2 - \lambda m_X^2)}.$$

Finally, I calculate the result of the propagator:

$$i\Pi^{\alpha\rho} = -\frac{i}{k^2 - m_X^2} g^{\alpha\rho} + \frac{i(1-\lambda)}{(k^2 - m_X^2)(k^2 - \lambda m_X^2)} k^\alpha k^\rho. \tag{2.21}$$

When $\lambda = 1$, it is called the Feynman gauge. When $\lambda = 0$, it is called the Unitary gauge. When $\lambda \to 0$ it is called the Landau gauge. Unfortunately, for massive vector bosons, the propagator depends upon the arbitrary gauge fixing parameter λ. In order to solve this problem, a gauge fixing condition is added to the Lagrangian, which results in new fields. The new fields are known as the Faddeev-Popov ghosts, named after Ludvig Faddeev and Victor Popov [15]. From the ghost Lagrangian, one can derive the propagators for the ghost fields. The ghost particles serve as amendments of the Feynman rules. Thanks to the $X^\pm$ model, the $GX^\pm$ can be implemented the same way as the ghost particles of SM gauge bosons with the additional coupling $\mu_{1,2}$ respectively. The detailed derivation and examples for the ghost fields can be found in *An Introduction to Quantum Field Theory* by Michael E. Peskin and Daniel V. Schroeder [31].

2.3 Kinematics

For a 2-body to 2-body scattering process with external momenta labeled as below;

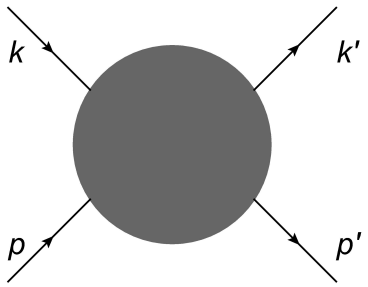

The Mandelstam variables are defined as [29]

$$\begin{aligned} s &= (p+p')^2 = (k+k')^2; \\ t &= (k-p)^2 = (k'-p')^2; \\ u &= (k'-p)^2 = (k-p')^2. \end{aligned} \tag{2.22}$$

Mandelstam variables have an identity of

$$s + t + u = m_1^2 + m_2^2 + m_3^2 + m_4^2. \tag{2.23}$$

Mandelstam variables are introduced to express the kinematic conditions of a 2-body to 2-body process in a Lorentz invariant way.

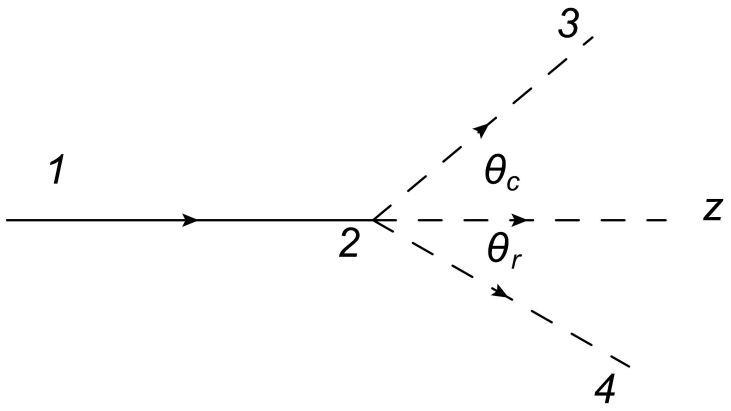

Figure 2.2: The kinematic schematic for a 2-body to 2-body scattering.

As a basic example, Figure 2.2 shows a 2-body to 2-body scattering. The known conditions are the masses of all four particles m_i (i=1,2,3,4), the energy of incoming particle E_1, its momentum p_1, the k_2 particle is at rest $p_2 = 0$ and the scattering angles

θ_c and θ_r.

$$\begin{aligned} k_1 &= (E_1, 0, 0, p_1), \\ k_2 &= (m, 0, 0, 0), \\ k_3 &= (E_3, p_3 \sin\theta_c, 0, p_3 \cos\theta_c), \\ k_4 &= (E_4, -p_4 \sin\theta_r, 0, p_4 \cos\theta_r). \end{aligned} \tag{2.24}$$

The conservation laws are

$$\begin{aligned} E_1 + E_2 &= E_3 + E_4, \\ p_3 \cos\theta_c + p_4 \cos\theta_r &= p_1, \\ p_3 \sin\theta_c &= -p_4 \sin\theta_r. \end{aligned} \tag{2.25}$$

Now the Mandelstam variables becomes

$$\begin{aligned} s &= (k_1 + k_2)^2 = m_1^2 + m_2^2 + 2(E_1 m_2 - 0) = m_1^2 + m_2^2 + 2E_1 m_2, \\ t &= (k_3 - k_1)^2 = (k_4 - k_2)^2 = m_4^2 + m_2^2 - 2E_4 m_2, \\ u &= (k_1 - k_4)^2 = (k_2 - k_3)^2 = m_2^2 + m_3^2 - 2E_3 m_2. \end{aligned} \tag{2.26}$$

Now we can write the kinematic conditions with s, t and u.

$$\begin{aligned} E_4 &= \frac{m_2^2 + m_4^2 - t}{2m_2}, \\ p_4 &= \sqrt{E_4^2 - m_4^2}, \\ E_3 &= \frac{m_2^2 + m_3^2 - u}{2m_2}, \\ p_3 &= \sqrt{E_3^2 - m_4^2}, \\ p_1 &= \sqrt{E_1^2 - m_1^2} \end{aligned} \tag{2.27}$$

We can do the same for the scattering angles,

$$t = (k_3 - k_1)^2 = m_3^2 + m_1^2 - 2E_1 E_3 + 2p_1 p_3 \cos\theta_c, \tag{2.28}$$

$$u = (k_4 - k_1)^2 = m_4^2 + m_1^2 - 2E_1E_4 + 2p_1p_4\cos\theta_r, \tag{2.29}$$

$$\cos\theta_c = \frac{t - m_1^2 - m_3^2 + 2E_1E_3}{2p_1p_3}, \tag{2.30}$$

$$\cos\theta_r = \frac{u - m_1^2 - m_4^2 + 2E_1E_4}{2p_1p_4}, \tag{2.31}$$

We can also write E_3 and p_3 as functions of E_1 and scattering angle θ_c

$$\begin{aligned} E_3 &= \frac{E_1}{1 + \frac{2E_1}{m_2}\sin^2\frac{\theta_c}{2}}, \\ p_3 &= \sqrt{E_3^2 - m_3^2}. \end{aligned} \tag{2.32}$$

Applying E_3 and p_3 to Eqn. 2.28 and 2.29 along with Eqn. 2.26 and 2.23, we can write s, t and u as a function of E_1 and θ_c, which are known kinematic conditions. Since a cross section can be expressed as a function of Mandelstam variables, it is a Lorentz invariant quantity.

Chapter 3

Higher Order Calculation

Feynman diagrams can represent all the possible processes for a scattering channel. In Figure 2.1, the Feynman diagram only contains one internal line, which is the simplest case among all the scattering patterns, known as the tree level/Born level Feynman diagram. In the actual physical interaction, there are more than one internal particle which require higher order Feynman diagrams to be represented. There is no limitation on the order of Feynman diagrams, as long as they follow basic conservation laws. In other words, any combination of a limited order of Feynman diagrams is only an approximation of the actual physical interaction.

The complexity of Feynman diagrams is closely associated with the calculation accuracy. More specifically, the order of the Feynman diagram is related to the order of approximation of the solution to the real cross section. The tree/leading order Feynman diagram dominates the cross section and each higher order brings more accuracy at the magnitude of the fine structure constant $\alpha = \frac{e^2}{4\pi\epsilon_0\hbar c} \approx \frac{1}{137}$. By convention, we set $c = \hbar = 1$, and hence e is also dimensionless. If one includes infinite orders of Feynman diagrams into the calculation, the overall probability of the scattering should be 1 - the sum of all the possibilities. Such a calculation is the exact solution to the true cross section. With such precision, one can predict the very nature of a particle scattering

process. However, it is impossible to include infinite orders of Feynman diagrams into calculation. In fact, the order of loop calculation is far from infinity, since the complexity of Feynman diagrams can escalate significantly as the order increases. In this research, the calculation accuracy is required to be at one loop level. At one loop level, there are two internal particles and the uncertainty level is at α

3.1 Regularization

Ultra Violet (UV) divergence causes mathematical breakdown in the integration, which jeopardizes the validity of Feynman calculus beyond tree level. However, as long as the mathematical model does not contain such integration breakdowns, then Feynman calculus should still be valid. The regularization consists of identifying the precise causes to UV divergences and introducing proper methods to avoid the integration breakdowns/divergences.

Mathematically speaking, regularization is the procedure to express the divergent terms explicitly and then "remove" them from the calculations by including the divergent term inside measurable values (e.g. bare masses and charges). The processed expression shall only consist of the physical measurable and the rearranged converged integral. The idea can be described in a generic equation:

$$\int \mathscr{M} = \int D + \int C = \text{Measurable} + \int C_{new}. \tag{3.1}$$

Physically, a propagating particle can interact with itself and the self interactions give divergent results at a specific order. If one includes all orders of self interaction, then the result shall be finite. This lies in the foundation of renormalization conditions. By calibrating the expression with the physical measurables, the divergence cancels. This

process is known as renormalization and will be discussed later in this chapter.

The integration boundaries of UV divergences are fixed and cause a 4th dimensional momentum (q) term in the denominator. In order to regularize the divergences, a dimension parameter D is introduced. Regularization scheme moves the integration into D(th) dimension, which means

$$d^4p \to d^Dp. \tag{3.2}$$

The regularization also requires a scalar parameter $\frac{\mu^{4-D}}{2\pi^D}$ is introduced to maintain the unit dimension as GeV. μ has a dimension of GeV

$$d^4q \quad (GeV^4) \to \mu^{4-D}d^Dq \quad (GeV^{4-D}GeV^D)$$

and the amplitude $\mathscr{M}$ becomes

$$\begin{aligned} \mathscr{M} &\propto \mu^{4-D} \int d\Omega \int \frac{dq \cdot q^{D-1}}{q^4} \\ &\propto \frac{q^{D-4}}{D-4}\Big|_0^\infty \end{aligned} \tag{3.3}$$

Let $D \to 4$,

$$\lim_{D\to 4} \frac{q^{D-4}}{D-4} = \lim_{D\to 4} \frac{q^0}{D-4} = \lim_{D\to 4} \frac{1}{D-4} \equiv \Delta. \tag{3.4}$$

Therefore, all UV divergent integrals can be written as a sum of regularized part $h\Delta$ and the initially converging part $f(s,t,u,m)$, where h is the coefficient of proportionality.

$$\mathscr{M} \propto \frac{h}{D-4} + f(s,t,u,m), \tag{3.5}$$

If Δ can be removed, the amplitude $\mathscr{M}$ will be convergent.

3.2 Amplitude Calculation

In Eqn. 2.4, one can separate the Dirac spinors/polarization vectors from the amplitude and leave the rest as a truncated graph. The Dirac spinors are always the same for all the Feynman diagrams of a single scattering channel. On the other hand, the truncated graphs are different from each other. They are based on the structures of internal interactions, which are the main focus in amplitude calculation. Once the truncated graphs are obtained, one can solve $\mathscr{M}^2$ with Dirac spinors using Casimir's trick [31]. The process is straight forward and can be found in *An Introduction to Quantum Field Theory* by Michael E. Peskin and Daniel V. Schroeder [31]. In this section, I derive the self-energy loop and triangle graphs using the methodology of Feynman rules for $X^{\pm}$ as described in Chapter 2, Feynman master integrals [31] and tensor decomposition [14]. Due to the nature of the box graphs, their evaluation is done using existing Mathematica packages FeynArts and FormCalc [20].

3.2.1 Fermion Self Energy Loop

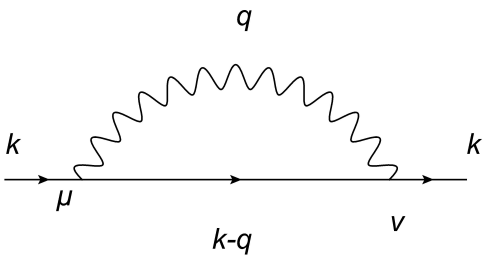

Figure 3.1: Feynman diagram for the ferimion self energy loop.

Using Feynman rules, one can obtain the truncated graph for the fermion self energy loop as

$$\begin{aligned}\Sigma(k) &= -ie^2 \int d^4q\, \gamma_\nu \frac{\not{k} - \not{q} + m}{(k-q)^2 - m^2} \gamma_\mu \frac{g^{\mu\nu}}{q^2} \\ &= 2ie^2 \underbrace{\int d^4q \frac{\not{k} - 2m}{[(k-q)^2 - m^2]q^2}}_{I_1} - 2ie^2 \underbrace{\int d^4q \frac{\not{q}}{[(k-q)^2 - m^2]q^2}}_{I_2}.\end{aligned} \tag{3.6}$$

The default integration limits for momentum q are from negative infinity to positive infinity. The first step is implementing dimensional regularization, which sets the integration dimension to D, instead of 4.

For convenience, this constant $\frac{\mu^{4-D}}{2\pi^D}$ will not be shown in the equations beyond this subsection.

For I_1,

$$I_1 = \frac{\mu^{4-D}}{2\pi^D} \int d^Dq \frac{1}{[(k-q)^2 - m^2]q^2}.$$

To further solve the integral, the Feynman trick is used

$$\frac{1}{ab} = \int_0^1 dz \frac{1}{[az + b(1-z)]^2}. \tag{3.7}$$

I_1 becomes

$$I_1 = \frac{\mu^{4-D}}{2\pi^D} \int_0^1 dz \int d^Dq \frac{1}{[(k-q)^2 z - m^2 z + q^2(1-z)]^2},$$

which can be rearranged to

$$I_1 = \frac{\mu^{4-D}}{2\pi^D} \int_0^1 dz \int d^Dq \frac{1}{[(q-kz)^2 - k^2z^2 + (k^2 - m^2)]^2}.$$

Due to the infinite integration limits, it does not affect the result with the shift $q - kz \to q$.

$$I_1 = \frac{\mu^{4-D}}{2\pi^D} \int_0^1 dz \int d^Dq \frac{1}{[q^2 - k^2z^2 + (k^2 - m^2)]^2}. \tag{3.8}$$

Now using the Feynman master integrals [31]:

$$\int \frac{d^D q}{2\pi^D} \frac{1}{(q^2-\Pi)^2} = \frac{i}{(4\pi)^{D/2}} \frac{\Gamma(2-\frac{D}{2})}{\Gamma(2)} \left(\frac{1}{\Pi}\right)^{2-\frac{D}{2}}. \tag{3.9}$$

$$I_1 = \frac{i\mu^{4-D}}{4\pi^D} \int_0^1 dz \frac{\Gamma\left(2-\frac{D}{2}\right)}{\Gamma(2)} \left(\frac{1}{q^2-k^2z^2+(k^2-m^2)}\right)^{2-\frac{D}{2}} dz,$$

where

$$\begin{aligned} \Gamma(z) &= \int_0^\infty t^{z-1} e^{-t} dt \\ &= \frac{1}{z} - \gamma + \theta(z). \end{aligned} \tag{3.10}$$

Here $\gamma \approx 0.5772$ is known as Euler Mascheroni constant. Therefore,

$$\Gamma\left(2-\frac{D}{2}\right) = \frac{2}{4-D} - \gamma + \theta\left(\frac{4-D}{2}\right)$$

or it can be expressed as

$$\Gamma\left(2-\frac{D}{2}\right) = \frac{2}{\epsilon} - \gamma + \theta\left(\epsilon\right)$$

where

$$4 - D = \epsilon.$$

In addition, one can also derive the following relationship,

$$\mu^{4-D} = (\mu^2)^{\frac{4-D}{2}} = 1 - \frac{\epsilon}{2} \ln\left(\frac{1}{\mu^2}\right) + \theta(4-D)$$

$$\left(\frac{1}{k^2z^2-(k^2-m^2)z}\right)^{\frac{\epsilon}{2}} = 1 - \frac{\epsilon}{2} \ln(k^2z^2 - k^2z + m^2z).$$

Note that ϵ approaches 0 when D is equal to 4, which is the limit for dimensional regularization. After rearranging the equation, we take the limit as $D \to 4$and integrate over dz. This is known as dimensional regularization, which confines the divergence into

the dimension.

$$I_1 = \frac{\mu^2}{(4\pi)^2 k^2}\left(\frac{2}{\epsilon} - \gamma + \frac{2k^2}{\mu^2} + \frac{m^2}{\mu^2}\ln\frac{m^2}{\mu^2} + \frac{k^2-m^2}{\mu^2}\ln\frac{k^2-m^2}{\mu^2}\right). \tag{3.11}$$

With a similar process and the fact that odd integrals of $\int d^D q \;\; f(q)$ are zero, we can solve for I_2. The only difference is that the numerator of I_2 is $\not{q} = \gamma^\mu q_\mu$ instead of 1. After the shift $q - kz \to q$, the numerator becomes $\not{q} + \not{k}z$. The $\not{q}$ component does not contribute because that part of I_2 is an odd integral, leaving only the $\not{k}$ dependent part left.

$$I_2 = \frac{\not{k}}{(4\pi)^2}\left[\frac{1}{\epsilon} - \frac{\gamma}{2} + 1 + \frac{m^2}{2k^2} - \frac{m^4}{2k^4}\ln\frac{m^2}{\mu^2} - \left(\frac{1}{2} - \frac{m^4}{2k^4}\right)\ln\frac{m^2-k^2}{\mu}\right]. \tag{3.12}$$

Overall, we solve the fermion self energy loop as

$$\begin{aligned}\Sigma(k) =& ie^2\frac{2ie^2\mu^2}{(4\pi)^2 k^2}\left(\frac{2}{\epsilon} - \gamma + \frac{2k^2}{\mu^2} + \frac{m^2}{\mu^2}\ln\frac{m^2}{\mu^2} + \frac{k^2-m^2}{\mu^2}\ln\frac{k^2-m^2}{\mu^2}\right) \\ &- \frac{2ie^2\not{k}}{(4\pi)^2}\left[\frac{1}{\epsilon} - \frac{\gamma}{2} + 1 + \frac{m^2}{2k^2} - \frac{m^4}{2k^4}\ln\frac{m^2}{\mu^2} - \left(\frac{1}{2} - \frac{m^4}{2k^4}\right)\ln\frac{m^2-k^2}{\mu}\right].\end{aligned} \tag{3.13}$$

3.2.2 Vector Boson Self Energy Loop

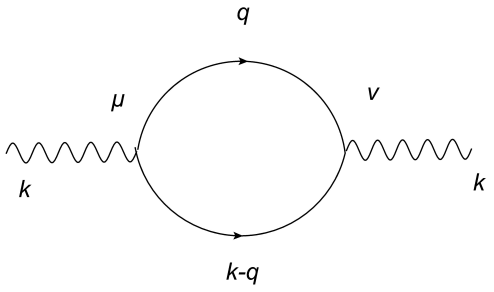

Figure 3.2: Feynman diagram for the vector boson self energy loop.

The truncated graph for the vector boson self energy loop is

$$B_{\mu\nu} = ie^2 \int d^D q \gamma_\nu \frac{\not{q} + m}{q^2 - m^2} \gamma_\mu \frac{\not{k} - \not{q} + m}{(k-q)^2 - m^2}. \tag{3.14}$$

Note that A_0, B_0 and C_0 can be solved easily using the same method to solve I_1 from the last subsection.

This expression essentially consists of the most simple amplitude integrals. The tensor decomposition technique can replace complex tensor integrals into a set of simple integrals through an algorithmic method. For example, a two point system of "second order" integral, based on the order of q in numerator, can be decomposed. The numerator of Eqn 3.14 is

$$\begin{aligned} \gamma_\nu(\not{q} + m)\gamma_\mu(\not{k} - \not{q}) =& \gamma_\nu \not{q} \gamma_\mu \not{k} - \gamma_\nu \not{q} \gamma_\mu \not{q} + m\gamma_\nu \gamma_\mu \not{k} \\ & - m\gamma_\nu \gamma_\mu \not{q} + m\gamma_\nu \not{q} + m^2 \gamma\nu\gamma_\mu, \end{aligned} \tag{3.15}$$

which contains 3 types of tensor integrals B_0, B_α and $B_{\alpha\beta}$. The relationship for these tensor integrals are [14]

$$B_\alpha = ie^2 \frac{\mu^{4-D}}{(2\pi)^3} \int d^D q \frac{q_\alpha}{[(q-k)^2 - m_1^2](q - m_2)^2}$$

$$B_{\alpha\beta} = ie^2 \frac{\mu^{4-D}}{(2\pi)^3} \int d^D q \frac{q_\alpha q_\beta}{[(q-k)^2 - m_1^2](q - m_2)^2}$$

and the corresponding tensor decompositions are [14]

$$B_\alpha = k_\alpha B_1$$

$$B_{\alpha\beta} = g_{\alpha\beta} B_{00} + k_\alpha k_\beta B_{11}.$$

The next step is using tensor reduction to break down these tensor structures into a basic expression. The basic expression resembles the linear algebra concept of

eigenvalues and eigenvectors

$$B_\alpha = k_\alpha B_1 = ie^2 \frac{\mu^{4-D}}{(2\pi)^3} \int d^D q \frac{q_\alpha}{[(k-q)^2 - m_1^2](q^2 - m_2^2)}.$$

After contracting both sides with k^α and dropping the constant coefficient in front, we get

$$\begin{aligned}
k^2 B_1 =& k_\alpha B_1 k^\alpha \\
=& \int d^D q \frac{q_\alpha k^\alpha}{[(k-q)^2 - m_1^2](q^2 - m_2^2)} \\
=& \frac{1}{2} \int d^D q \frac{2kq}{[(k-q)^2 - m_1^2](q^2 - m_2^2)} \\
=& -\frac{1}{2} \int d^D q \frac{[(k-q)^2 - m_1^2] - (k^2 - m_1^2) - (q^2 - m_2^2) - m_2^2}{[(k-q)^2 - m_1^2](q^2 - m_2^2)} \\
=& -\frac{1}{2} \left(\underbrace{\int d^D q \frac{1}{q^2 - m_2^2}}_{A_0(m_2^2)} - (k^2 - m_1^2 + m_2^2) \underbrace{\int d^D q \frac{1}{[(k-q)^2 - m_1^2](q^2 - m_2^2)}}_{B_0(k, m_1, m_2)} - \right. \\
& \left. - \underbrace{\int d^D q \frac{1}{(k-q)^2 - m_1^2}}_{A_0(m_1)} \right).
\end{aligned} \tag{3.16}$$

By comparing this to the tensor decomposition result, we can solve

$$B_1 = -\frac{1}{2k^2}[A_0(m_2) - A_0(m_1) - (k^2 - m_1^2 + m_2^2) B_0(k, m_1, m_2)]. \tag{3.17}$$

The next step is to solve B_{11} and B_{00}. Start from

$$\begin{aligned}
B_{\alpha\beta} g^{\alpha\beta} &= g_{\alpha\beta} g^{\alpha\beta} B_{00} + g^{\alpha\beta} k_\alpha k_\beta B_{11} \\
&= 4 B_{00} + k^2 B_{11}
\end{aligned} \tag{3.18}$$

and

$$B_{\alpha\beta}k^{\alpha} = k_{\beta}B_{00} + k^2 k_{\beta}B_{11}. \tag{3.19}$$

Using the integral form of Eqn. 3.18, we can solve

$$\begin{aligned} B_{\alpha\beta}g^{\alpha\beta} &= \int d^D q \frac{q^2 - m_2^2 + m_2^2}{[(k-q)^2 - m_1^2](q^2 - m_2^2)} \\ &= \int d^D q \frac{1}{(k-q)^2 - m_1^2} + m_2^2 \int d^D q \frac{1}{[(k-q)^2 - m_1^2](q^2 - m_2^2)} \\ &= A_0(m_1) + m_2^2 B_0(k, m_1, m_2) = 4B_{00} + k^2 B_{11}. \end{aligned} \tag{3.20}$$

Using the integral form of Eqn. 3.19, we can solve

$$\begin{aligned} B_{\alpha\beta}k^{\alpha} &= \int d^D q \frac{(kq)q_{\beta}}{[(k-q)^2 - m_1^2](q^2 - m_2^2)} \\ &= -\frac{1}{2}\int d^D q \; q_{\beta} \frac{[(k-q)^2 - m_1^2] - (k^2 - m_1^2) - (q^2 - m_2^2) - m_2^2}{[(k-q)^2 - m_1^2](q^2 - m_2^2)} \\ &= \underbrace{-\frac{1}{2}\int d^D q \frac{q_{\beta}}{q^2 - m_2^2}}_{0} + \frac{1}{2}\int d^D q \frac{q_{\beta}(k^2 - m_1^2 + m_2^2)}{[(k-q)^2 - m_1^2](q^2 - m_2^2)} + \underbrace{\frac{1}{2}\int d^D q \frac{q_{\beta}}{(k-q)^2 - m_1^2}}_{\frac{1}{2}\int d^D q \frac{q_{\beta}+k_{\beta}}{q^2 - m_1^2}} \\ &= \frac{1}{2}\int d^D q \frac{q_{\beta}(k^2 - m_1^2 + m_2^2)}{[(k-q)^2 - m_1^2](q^2 - m_2^2)} + \underbrace{\frac{1}{2}\int d^D q \frac{q_{\beta}}{q^2 - m_2^2}}_{0} + \frac{1}{2}\int d^D q \frac{k_{\beta}}{q^2 - m_1^2} \\ &= \frac{1}{2}(k^2 - m_1^2 + m_2^2)k_{\beta}B_1 + \frac{1}{2}k_{\beta}A_0(m_2^2) = k_{\beta}B_{00} + k^2 k_{\beta}B_{11}. \end{aligned} \tag{3.21}$$

Therefore

$$B_{00} + k^2 B_{11} = \frac{1}{2}[(k^2 - m_1^2 + m_2^2)B_1 + A_0(m_2)]. \tag{3.22}$$

Now we can solve B_{00} and B_{11} from Eqn. 3.20 and 3.22

$$B_{11} = \frac{1}{k^2}\left(\frac{2(k^2 - m_1^2 + m_2^2)}{3}B_1 + \frac{1}{3}\left(2A_0(m_2) - A_0(m_1)\right) - \frac{1}{3}m_2^2 B_0(k, m_1, m_2)\right); \tag{3.23}$$

$$B_{00} = \frac{1}{6}\left(2A_0(m_1) - A_0(m_2)\right) + \frac{1}{3}m_2^2 B_0 - \frac{1}{6}(k^2 - m_1^2 + m_2^2)B_1. \tag{3.24}$$

3.2.3 Triangle Graphs

Triangle graphs are three points integrals, which requires a more advanced tensor decomposition approach.

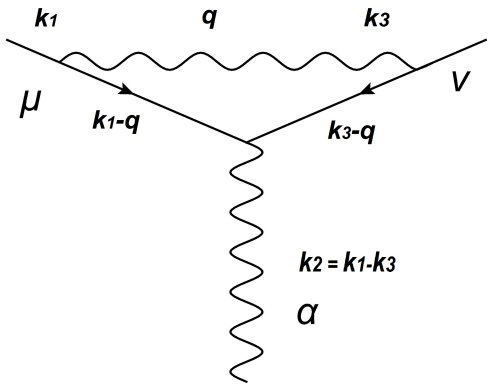

Figure 3.3: Example Feynman diagram of a triangle graph.

As an example, we will show a QED type of the vertex correction graph

$$C_\alpha = ie^3 \int d^D q \gamma_\nu \frac{\not{k}_3 - \not{q} + m}{(k_3 - q)^2 - m^2} \gamma_\alpha \frac{\not{k}_1 - \not{q} + m}{(k_1 - q)^2 - m^2} \gamma_\mu \frac{g_{\mu\nu}}{q^2 - \lambda^2}. \tag{3.25}$$

Here λ is introduced as an infrared cutoff to deal with the infrared divergence caused by the massless photon. The numerator becomes

$$\begin{aligned} \gamma_\nu(\not{k}_3 - \not{q} + m)\gamma_\alpha(\not{k}_1 - \not{q} + m)\gamma^\nu = &\gamma_\nu \not{k}_3 \gamma_\alpha \not{k}_1 \gamma^\nu - \gamma_\nu \not{q} \gamma_\alpha \not{k}_1 \gamma^\nu + \gamma_\nu m \gamma_\alpha \not{k}_1 \gamma^\nu \\ &- \gamma_\nu \not{k}_3 \gamma_\alpha \not{q} \gamma^\nu + \gamma_\nu \not{q} \gamma_\alpha \not{q} \gamma^\nu - \gamma_\nu m \gamma_\alpha \not{q} \gamma_\nu \\ &m\gamma_\nu \not{k}_3 \gamma_\alpha \gamma^\nu - m\gamma_\nu \not{q} \gamma_\alpha \gamma^\nu + m^2 \gamma_\nu \gamma_\alpha \gamma^\nu, \end{aligned} \tag{3.26}$$

which consists of 3 types of tensor integrals C_0, C_α and $C_{\alpha\beta}$ [14].

$$C_\alpha = k_{1\alpha} C_1 + k_{2\alpha} C_2$$

$$C_{\alpha\beta} = g_{\alpha\beta} C_{00} + k_{1\alpha} k_{1\beta} C_{11} + k_{2\alpha} k_{2\beta} C_{22} + k_{1\alpha} k_{2\beta} C_{12} + k_{1\beta} k_{2\alpha} C_{21}.$$

Meanwhile the C_0 can be solved using the previous technique shown in the fermion self energy loop.

$$C_0 = \int d^D q \frac{1}{\underbrace{\left((k_3-q)^2-m^2\right)}_{D_3}\underbrace{\left((k_1-q)^2-m^2\right)}_{D_1}\underbrace{\left(q^2-\lambda^2\right)}_{D_0}}. \tag{3.27}$$

D_0,D_1,D_3 are introduced for convenience. The main difference is that now the integral needs the higher order Feynman trick.

$$\frac{1}{abc} = 2\int_0^1 dxdy \frac{1}{xa+yb+(1-x-y)c}$$

$$\begin{aligned} C_0 &= \int d^D q \int_0^1 dxdy \frac{2}{x((k_3-q)^2-m^2)+y\left((k_1-q)^2-m^2\right)+(1-x-y)\left(q^2-\lambda^2\right)} \\ &= \int d^D q \int_0^1 dxdy \frac{2}{\underbrace{(q-xk_3-yk_1)^2}_{q-xk_3-yk_1\to q} - (xk_3+yk_1)^2-(1-x-y)\lambda^2} \\ &= \int d^D q \int_0^1 dxdy \frac{2}{q^2-\underbrace{\left[(xk_3+yk_1)^2+(1-x-y)\lambda^2\right]}_{\Pi}}. \end{aligned} \tag{3.28}$$

With the same Feynman master integral and different Π.

$$\int \frac{d^D q}{2\pi^D}\frac{1}{(q^2-\Pi)^2} = \frac{i}{(4\pi)^{D/2}}\frac{\Gamma(2-\frac{D}{2})}{\Gamma(2)}\left(\frac{1}{\Pi}\right)^{2-\frac{D}{2}}$$

The rest of the procedure is identical to the one used after Eqn. 3.9.

The next step is to solve first order tensor integral C_β

$$C_\beta = k_{1\beta}C_1 + k_{3\beta}C_3 = \int d^D q \frac{q_\beta}{D_0 D_1 D_3} \tag{3.29}$$

Now we contract Eqn. 3.29 with k_1^β and k_3^β and note that $k_1^2 = k_3^2 = m^2$

$$J_1 = C_\beta k_1^\beta = \int d^D q \frac{qk_1}{D_0 D_1 D_3} = m^2 C_1 + (k_1 k_3) C_3, \tag{3.30}$$

$$J_2 = C_\beta k_3^\beta = \int d^D q \frac{qk_3}{D_0 D_1 D_3} = (k_1 k_3) C_1 + m^2 C_3. \tag{3.31}$$

Now we can write these two equations as a system

$$\begin{aligned} a_{11} C_1 + a_{12} C_3 &= J_1 \\ a_{21} C_1 + a_{22} C_3 &= J_3, \end{aligned} \tag{3.32}$$

with

$$\begin{aligned} a_{11} &= a_{22} = m^2; \\ a_{21} &= a_{12} = (k_1 k_3); \end{aligned} \tag{3.33}$$

which can be solved as

$$\begin{aligned} C_1 &= \frac{\begin{vmatrix} J_1 & a_{12} \\ J_3 & a_{22} \end{vmatrix}}{G}, \\ C_3 &= \frac{\begin{vmatrix} a_{11} & J_1 \\ a_{21} & J_3 \end{vmatrix}}{G}, \end{aligned} \tag{3.34}$$

where

$$G = \begin{vmatrix} a_{11} & a_{12} \\ a_{21} & a_{22} \end{vmatrix} = m^4 - (k_1 k_3)^2$$

is known as the Gramm determinant. Note that $(k_1^\mu k_{3\mu}) = (k_1 k_3)$ represents a dot

product. Therefore, $(k_1k_3)^2 \neq k_1^2k_3^2$.

$$\begin{aligned} C_1 &= \frac{1}{m^4-(k_1k_3)^2}(m^2J_1-(k_1k_3)J_3), \\ C_3 &= \frac{1}{m^4-(k_1k_3)^2}(m^2J_3-(k_1k_3)J_1). \end{aligned} \tag{3.35}$$

The next step is to solve J_1,

$$\begin{aligned} J_1 &= \int d^Dq \frac{(qk_1)}{D_0D_3[(k_1-q)^2-m^2]} \\ &= -\frac{1}{2}\int d^Dq \frac{[(k_1-q)^2-m^2]+m^2-k_1^2-q^2}{D_0D_3[(k_1-q)^2-m^2]} \\ &= -\frac{1}{2}\int d^Dq \left(\frac{1}{D_0D_3}-\frac{q^2-\lambda^2}{D_0D_1D_3}-\frac{\lambda^2}{D_0D_1D_3}\right) \\ &= -\frac{1}{2}\left[B_0(k_3,\lambda,m)-B_0(k_1-k_3,m,m)-\lambda^2C_0(k_1,k_3,\lambda,m,m)\right]. \end{aligned} \tag{3.36}$$

Note that when $\lambda^2 \to 0$, which is the cutoff limit for λ, λ^2C_0 approaches 0.

Similarly, we can solve J_2

$$J_2 = -\frac{1}{2}\left[B_0(k_1,\lambda,m)-B_0(k_3,k_1,m)-\lambda^2C_0(k_1,k_3,\lambda,m,m)\right]. \tag{3.37}$$

Finally, for the second order tensor $C_{\delta\beta}$

$$\begin{aligned} C_{\delta\beta} &= g_{\delta\beta}C_{00}+k_{1\delta}k_{1\beta}C_{11}+k_{3\delta}k_{3\beta}C_{33}+k_{1\delta}k_{3\beta}C_{13}+k_{1\beta}k_{3\delta}C_{31} \\ &= g_{\delta\beta}C_{00}+k_{1\delta}k_{1\beta}C_{11}+k_{3\delta}k_{3\beta}C_{33}+(k_{1_\delta}k_{3\beta}+k_{1\beta}k_{3\delta})C_{13}. \end{aligned} \tag{3.38}$$

$k_1^2 = k_3^2 = m^2$ leads to $C_{13} = C_{31}$

$$k_{1_\delta}k_{3\beta}C_{13}+k_{1\beta}k_{3\delta}C_{31} = (k_{1_\delta}k_{3\beta}+k_{1\beta}k_{3\delta})C_{13}.$$

Contract $C_{\delta\beta}$ with $g^{\delta\beta}$, $k_1^\delta k_3^\beta$, $k_1^\delta k_1^\beta$ and $k_3^\delta k_3^\beta$ respectively

$$
\begin{aligned}
T_1 = C_{\delta\beta} g^{\delta\beta} &= 4C_{00} + m^2 C_{11} + m^2 C_{33} + 2(k_1 k_3) C_{13} \\
&= \int d^D q \frac{q_\delta q_\beta g^{\delta\beta}}{D_0 D_1 D_3} \\
&= \int d^D q \frac{q^2}{D_0 D_1 D_3} \\
&= \int d^D q \frac{(q^2 - \lambda^2) + \lambda^2}{D_0 D_1 D_3} \\
&= \int d^D q \frac{1}{D_1 D_3} + \lambda^2 \int d^D q \frac{1}{D_0 D_1 D_3} \\
&= B_0(k_1 - k_3, m, m) + \lambda^2 C_0(k_1, k_3, \lambda, m, m);
\end{aligned}
\tag{3.39}
$$

$$
\begin{aligned}
T_2 =& C_{\delta\beta} k_1^\delta k_3^\beta = C_{\delta\beta} k_3^\delta k_1^\beta \\
=& (k_1 k_3) C_{00} + m^2 (k_1 k_3)(C_{11} + C_{33}) + [m^4 + (k_1 k_3)^2] C_{13} \\
=& \int d^D q \frac{q_\delta q_\beta k_1^\delta k_3^\beta}{D_0 D_1 D_3} \\
=& \int d^D q \frac{(qk_1)(qk_3)}{D_0 D_1 D_3} \\
=& -\frac{1}{2} \int d^D q \left(\frac{(qk_3)}{D_0 D_3} - \frac{D_0 (qk_3)}{D_0 D_1 D_3} - \frac{\lambda^2 (qk_3)}{D_0 D_1 D_3} \right) \\
=& \frac{1}{4} \int d^D q \left(\frac{[(k_3 - q)^2 - m^2] - q^2}{D_0 D_3} - \frac{[(k_3 - q)^2 - m^2] - q^2}{D_1 D_3} - \lambda^2 \frac{[(k_3 - q)^2 - m^2] - q^2}{D_0 D_1 D_3} \right) \\
=& \underbrace{\frac{1}{4} \int d^D q \left(\frac{1}{D_0} - \frac{1}{D_3} - \frac{\lambda^2}{D_0 D_3} \right)}_{T_{21}} - \underbrace{\frac{1}{4} \int d^D q \left(\frac{1}{D_1} - \frac{(q + k_1)^2}{(q^2 - m^2)((q - k_3 + k_1)^2 - m^2)} \right)}_{T_{22}} \\
& - \underbrace{\lambda^2 \frac{1}{4} \int d^D q \left(\frac{[(k_3 - q)^2 - m^2] - q^2}{D_0 D_1 D_3} \right)}_{T_{23}};
\end{aligned}
\tag{3.40}
$$

We can obtain

$$
T_{21} = \frac{1}{4}(A_0(\lambda) - A_0(k_3, m) - \lambda^2 B_0(k_3, m, \lambda)), \tag{3.41}
$$

and

$$\begin{aligned}
T_{22} &= \frac{1}{4}\int d^D q \left[\frac{1}{D_1} - \frac{1}{D_3} - \frac{2(k_1 q)}{D_1 D_3}\right] \\
&= \frac{1}{4}\left(A_0(m) - A_0(m) - 2k_{1,\alpha}\int d^D q \frac{q^\alpha}{[(k_1-q)^2-m^2][(k_3-q)^2-m^2]}\right) \\
&= -\frac{1}{2}k_{1\alpha}\int d^D q \frac{k_1^\alpha + q^\alpha}{(q^2-m^2)[(q+k_3-k_1)^2-m^2]} \\
&= -\frac{1}{2}m^2\int d^D q \frac{1}{(q^2-m^2)[(q-k_1+k_3)^2-m^2]} - \frac{1}{2}m^2 B_1(k_1-k_3,m,m) \\
&= -\frac{1}{2}m^2(B_0(k_1-k_3,m,m) + B_1(k_1-k_3,m,m)),
\end{aligned} \tag{3.42}$$

$$\begin{aligned}
T_{23} &= \frac{\lambda^2}{4}\int d^D q \frac{[(k_3-q)^2-m^2]-q^2}{D_0 D_1 D_3} \\
&= \frac{\lambda^2}{4}\int d^D q \left(\frac{1}{D_0 D_1} - \frac{q^2-\lambda^2+\lambda^2}{D_0 D_1 D_3}\right) \\
&= \frac{\lambda^2}{4}(B_0(k_1,\lambda,m) - B_0(k_1-k_3,m,m) - \lambda^2 C_0(k_1,k_3,\lambda,m,m)).
\end{aligned} \tag{3.43}$$

As a result,

$$\begin{aligned}
T_2 &= T_{21} - T_{22} - T_{23} \\
&= \frac{1}{4}(A_0(\lambda) - A_0(k_3,m) - \lambda^2 B_0(k_3,m,\lambda)) + \frac{1}{2}m^2(B_0(k_1-k_3,m,m) + B_1(k_1-k_3,m,m)) \\
&\quad - \frac{\lambda^2}{4}(B_0(k_1,\lambda,m) - B_0(k_1-k_3,m,m) - \lambda^2 C_0(k_1,k_3,\lambda,m,m)).
\end{aligned} \tag{3.44}$$

As the next piece of the puzzle,

$$
\begin{aligned}
T_3 &= C_{\delta\beta}k_1^\delta k_1^\beta \\
&= m^2 C_{00} + m^2 C_{11} + (k_1 k_3)^2 C_{33} + 2m^2(k_1 k_3)C_{13} \\
&= \int d^D q \frac{q_\delta q_\beta k_1^\delta k_1^\beta}{D_0 D_1 D_3} \\
&= \int d^D q \frac{(qk_1)^2}{D_0 D_1 D_3} \\
&= -\frac{1}{2}\int d^D q \left(\frac{(qk_1)}{D_0 D_3} - \frac{D_0(qk_1)}{D_0 D_1 D_3} - \frac{\lambda^2(qk_1)}{D_0 D_1 D_3}\right) \\
&= \frac{1}{4}\int d^D q \left(\frac{(qk_1)}{D_0 D_3} - \frac{[(k_1-q)^2-m^2]-q^2}{D_1 D_3} - \lambda^2\frac{[(k_1-q)^2-m^2]-q^2}{D_0 D_1 D_3}\right) \\
&= \underbrace{\frac{1}{4}[m^2 B_1(k_3,m,\lambda)]}_{T_{31}} - \underbrace{\frac{1}{4}\int d^D q \left(\frac{1}{D_3} - \frac{(q+k_1)^2}{(q^2-m^2)((q-k_3+k_1)^2-m^2)}\right)}_{T_{32}} \\
&\quad - \underbrace{\lambda^2\frac{1}{4}\int d^D q \left(\frac{[(k_1-q)^2-m^2]-q^2}{D_0 D_1 D_3}\right)}_{T_{33}}.
\end{aligned}
\tag{3.45}
$$

Similar to the process to solve T_2, one can obtain

$$
\begin{aligned}
T_{32} &= \frac{1}{4}\int d^D q \left[\frac{1}{D_3} - \frac{1}{D_3} - \frac{2(k_1 q)}{D_1 D_3}\right] \\
&= \frac{1}{4}\left(A_0(m) - A_0(m) - 2k_{1,\alpha}\int d^D q \frac{q^\alpha}{[(k_1-q)^2-m^2][(k_3-q)^2-m^2]}\right) \\
&= -\frac{1}{2}k_{1\alpha}\int d^D q \frac{k_1^\alpha + q^\alpha}{(q^2-m^2)[(q+k_3-k_1)^2-m^2]} \\
&= -\frac{1}{2}m^2\int d^D q \frac{1}{(q^2-m^2)[(q-k_1+k_3)^2-m^2]} - \frac{1}{2}m^2 B_1(k_1-k_3,m,m) \\
&= -\frac{1}{2}m^2(B_0(k_1-k_3,m,m) + B_1(k_1-k_3,m,m)),
\end{aligned}
\tag{3.46}
$$

$$
\begin{aligned}
T_{33} &= \frac{\lambda^2}{4}\int d^D q \frac{[(k_1-q)^2-m^2]-q^2}{D_0 D_1 D_3} \\
&= \frac{\lambda^2}{4}\int d^D q \left(\frac{1}{D_0 D_3} - \frac{q^2-\lambda^2+\lambda^2}{D_0 D_1 D_3}\right) \\
&= \frac{\lambda^2}{4}(B_0(k_3,\lambda,m) - B_0(k_1-k_3,m,m) - \lambda^2 C_0(k_1,k_3,\lambda,m,m)).
\end{aligned}
\tag{3.47}
$$

Therefore,

$$\begin{aligned} T_3 = &\frac{1}{4}(m^2 B_1(k_3, m, \lambda)) + \frac{1}{2}m^2(B_0(k_1 - k_3, m, m) + B_1(k_1 - k_3, m, m)) \\ &- \frac{\lambda^2}{4}(B_0(k_3, \lambda, m) - B_0(k_1 - k_3, m, m) - \lambda^2 C_0(k_1, k_3, \lambda, m, m)). \end{aligned} \tag{3.48}$$

$$\begin{aligned} T_4 =& C_{\delta\beta}k_3^\delta k_3^\beta \\ =& m^2 C_{00} + (k_1 k_3)^2 C_{11} + m^2 C_{33} + 2m^2(k_1 k_3)C_{13} \\ =& \int d^D q \frac{q_\delta q_\beta k_1^\delta k_1^\beta}{D_0 D_1 D_3} \\ =& \int d^D q \frac{(qk_3)^2}{D_0 D_1 D_3} \\ =& -\frac{1}{2}\int d^D q \left(\frac{(qk_3)}{D_0 D_1} - \frac{D_0(qk_3)}{D_0 D_1 D_3} - \frac{\lambda^2(qk_3)}{D_0 D_1 D_3}\right) \\ =& \frac{1}{4}\int d^D q \left(\frac{(qk_3)}{D_0 D_1} - \frac{[(k_3 - q)^2 - m^2] - q^2}{D_1 D_3} - \lambda^2 \frac{[(k_3 - q)^2 - m^2] - q^2}{D_0 D_1 D_3}\right) \\ =& \underbrace{\frac{1}{4}[m^2 B_1(k_1, m, \lambda)]}_{T_{41}} - \underbrace{\frac{1}{4}\int d^D q \left(\frac{1}{D_1} - \frac{(q + k_1)^2}{(q^2 - m^2)((q - k_3 + k_1)^2 - m^2)}\right)}_{T_{42}} \\ &- \underbrace{\lambda^2 \frac{1}{4}\int d^D q \left(\frac{[(k_3 - q)^2 - m^2] - q^2}{D_0 D_1 D_3}\right)}_{T_{43}}, \end{aligned} \tag{3.49}$$

Applying the same technique,

$$\begin{aligned} T_{42} &= \frac{1}{4}\int d^D q \left[\frac{1}{D_1} - \frac{1}{D_3} - \frac{2(k_1 q)}{D_1 D_3}\right] \\ &= \frac{1}{4}\left(A_0(m) - A_0(m) - 2k_{1,\alpha}\int d^D q \frac{q^\alpha}{[(k_1 - q)^2 - m^2][(k_3 - q)^2 - m^2]}\right) \\ &= -\frac{1}{2}k_{1\alpha}\int d^D q \frac{k_1^\alpha + q^\alpha}{(q^2 - m^2)[(q + k_3 - k_1)^2 - m^2]} \\ &= -\frac{1}{2}m^2 \int d^D q \frac{1}{(q^2 - m^2)[(q - k_1 + k_3)^2 - m^2]} - \frac{1}{2}m^2 B_1(k_1 - k_3, m, m) \\ &= -\frac{1}{2}m^2(B_0(k_1 - k_3, m, m) + B_1(k_1 - k_3, m, m)), \end{aligned} \tag{3.50}$$

$$\begin{aligned} T_{43} &= \frac{\lambda^2}{4}\int d^D q \frac{[(k_3-q)^2-m^2]-q^2}{D_0 D_1 D_3} \\ &= \frac{\lambda^2}{4}\int d^D q \left(\frac{1}{D_0 D_1} - \frac{q^2-\lambda^2+\lambda^2}{D_0 D_1 D_3}\right) \\ &= \frac{\lambda^2}{4}(B_0(k_1,\lambda,m) - B_0(k_1-k_3,m,m) - \lambda^2 C_0(k_1,k_3,\lambda,m,m)). \end{aligned} \tag{3.51}$$

This becomes,

$$\begin{aligned} T_4 = \frac{1}{4}(m^2 B_1(k_3,m,\lambda)) + \frac{1}{2}m^2(B_0(k_1-k_3,m,m) + B_1(k_1-k_3,m,m)) \\ - \frac{\lambda^2}{4}(B_0(k_1,\lambda,m) - B_0(k_1-k_3,m,m) - \lambda^2 C_0(k_1,k_3,\lambda,m,m)). \end{aligned} \tag{3.52}$$

Now we have Eqn.3.39, Eqn.3.44, Eqn.3.48 and Eqn.3.52 involving T_1 to T_4 and 4 unknowns C_{00}, C_{11}, C_{33} and C_{13}.

$$T_1 = 4C_{00} + m^2 C_{11} + m^2 C_{33} + 2(k_1 k_3) C_{13},$$

$$T_2 = (k_1 k_3) C_{00} + m^2 (k_1 k_3)(C_{11} + C_{33}) + [m^4 + (k_1 k_3)^2] C_{13},$$

$$T_3 = m^2 C_{00} + m^2 C_{11} + (k_1 k_3)^2 C_{33} + 2m^2 (k_1 k_3) C_{13},$$

$$T_4 = m^2 C_{00} + (k_1 k_3)^2 C_{11} + m^2 C_{33} + 2m^2 (k_1 k_3) C_{13}.$$

One can solve this system of equations for C_{00}, C_{11}, C_{13} and C_{33}, using Cramer's rule.

3.2.4 Box Graphs

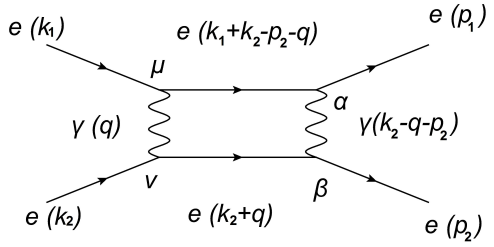

Figure 3.4: Feynman diagram for a box graph of Möller scattering.

As 4 point integrals, the truncated box graphs have complicated structures. Therefore, only one specific box graph is picked as an example, as shown in Figure 3.4, whose expression is

$$D = ie^4 \int d^4q \gamma_\alpha \frac{\not{k}_1 + \not{k}_2 - \not{p}_2 - \not{q} + m_e}{(-k_1 - k_2 + p_2 + q)^2 - m_e^2} \gamma_\mu \frac{g^{\mu\nu}}{q^2} \gamma_\nu \frac{\not{k}_2 + \not{q} + m_e}{(k_2 + q_2)^2 - m_e^2} \gamma_\beta \frac{g^{\alpha\beta}}{(q + p_2 - k_2)^2}. \tag{3.53}$$

Using the tensor integral decomposition for 4 point graphs[14],

$$D^\alpha = \sum_{i_1=1}^{3} k_{i_1}^\mu D_{1i},$$

$$D^{\alpha\beta} = \sum_{i_1,i_2=1}^{3} k_{i_1}^\alpha k_{i_2}^\beta D_{i_1,i_2} + g^{\alpha\beta} D_{00}.$$

Using the same tensor decomposition reduction technique, the expression for the

box graph is

$$
\begin{aligned}
D =&\alpha^2[(D_{11}+2D_{13}+D_3+D_{33})[\not{k}_1\omega^+ f_{\mu\nu}][\not{k}_1\omega^+ f^{\mu\nu}] \\
&-(2D_{13}+D_2+2D_{23}+D_3)[\not{k}_1\omega^+ f_{\mu\nu}][\not{k}_2\omega^+ f^{\mu\nu}] \\
&+(D_{11}+D_{22})[\not{k}_2\omega^+ f_{\mu\nu}][\not{k}_2\omega^+ f^{\mu\nu}]-(2D_{11}+D_{13})[\not{k}_1\omega^+ f_{\mu\nu}][\not{k}_3\omega^+ f_{\mu\nu}] \\
&+2D_{12}[\not{k}_2\omega^+ f_{\mu\nu}][\not{k}_3\omega^+ f_{\mu\nu}]+D_{11}[\not{k}_3\omega^+ f_{\mu\nu}][\not{k}_3\omega^+ f^{\mu\nu}]+D_{00}[\omega^+ f_{\mu\nu}\gamma_\alpha][\omega^+ f^{\mu\nu}\gamma^\alpha] \\
&+(2D_{11}+4D_{12}+2D_2+2D_{33})[\not{k}_1\omega^+ f_{\mu\nu}][\omega^-\not{k}_1 f^{\mu\nu}] \\
&-(2D_{12}+D_2+2D_{23}+D_2)[\not{k}_2\omega^+ f_{\mu\nu}][\omega^-\not{k}_1 f^{\mu\nu}] \\
&-(2D_{11}+2D_{12})[\not{k}_3\omega^+ f_{\mu\nu}][\omega^-\not{k}_1 f^{\mu\nu}] \\
&+(D_{11}+2D_{12}+D_2+D_{33})[\omega^-\not{k}_1 f_{\mu\nu}][\omega^-\not{k}_1 f^{\mu\nu}] \\
&-(2D_{12}+D_2+2D_{23}+D_2)[\not{k}_1\omega^+ f_{\mu\nu}][\omega^-\not{k}_2 f^{\mu\nu}] \\
&+(2D_2+2D_{22})[\not{k}_2\omega^+ f_{\mu\nu}][\omega^-\not{k}_2 f^{\mu\nu}] \\
&+2D_{12}[\not{k}_3\omega^+ f_{\mu\nu}][\omega^-\not{k}_2 f^{\mu\nu}])-(2D_{12}+D_2+2D_{23}+D_2)[\omega^-\not{k}_1 f_{\mu\nu}][\omega^-\not{k}_2 f^{\mu\nu}] \\
&-D_0)([\not{k}_1\omega^+ f_{\mu\nu}][\not{k}_2\omega^+ f^{\mu\nu}]+[\not{k}_2\omega^+ f_{\mu\nu}][\omega^-\not{k}_1 f^{\mu\nu}]+[\not{k}_1\omega^+ f_{\mu\nu}][\omega^-\not{k}_2 f^{\mu\nu}] \\
&+[\omega^-\not{k}_1 f_{\mu\nu}][\omega^-\not{k}_2 f^{\mu\nu}]+(D_2+D_{22})[\omega^-\not{k}_2 f_{\mu\nu}][\omega^-\not{k}_2 f^{\mu\nu}] \\
&-(2D_{11}+2D_{12})[\not{k}_1\omega^+ f_{\mu\nu}][\omega^-\not{k}_3 f^{\mu\nu}]2D_{12}[\not{k}_2\omega^+ f_{\mu\nu}][\omega^-\not{k}_3 f^{\mu\nu}] \\
&+2D_{11}[\not{k}_3\omega^+ f_{\mu\nu}][\omega^-\not{k}_3 f^{\mu\nu}]-(2D_{11}+2D_{12})[\omega^-\not{k}_1 f_{\mu\nu}][\omega^-\not{k}_3 f^{\mu\nu}] \\
&-D_1(-[\not{k}_1\omega^+ f_{\mu\nu}][\not{k}_1\omega^+ f^{\mu\nu}] \\
&+[\not{k}_1\omega^+ f_{\mu\nu}][\not{k}_2\omega^+ f^{\mu\nu}]+[\not{k}_1\omega^+ f_{\mu\nu}][\not{k}_3\omega^+ f^{\mu\nu}] \\
&-[\not{k}_2\omega^+ f_{\mu\nu}][\not{k}_3\omega^+ f^{\mu\nu}]-2[\not{k}_1\omega^+ f_{\mu\nu}][\omega^-\not{k}_1 f^{\mu\nu}]+[\not{k}_2\omega^+ f_{\mu\nu}][\omega^-\not{k}_1 f^{\mu\nu}] \\
&+[\not{k}_3\omega^+ f_{\mu\nu}][\omega^-\not{k}_1 f^{\mu\nu}]-[\omega^-\not{k}_1 f_{\mu\nu}][\omega^-\not{k}_1 f^{\mu\nu}])+[\not{k}_1\omega^+ f_{\mu\nu}][\omega^-\not{k}_2 f^{\mu\nu}] \\
&-[\not{k}_3\omega^+ f_{\mu\nu}][\omega^-\not{k}_2 f^{\mu\nu}]+[\omega^-\not{k}_1 f_{\mu\nu}][\omega^-\not{k}_2 f^{\mu\nu}] \\
&+[\not{k}_1\omega^+ f_{\mu\nu}][\omega^-\not{k}_3 f^{\mu\nu}]-[\not{k}_2\omega^+ f_{\mu\nu}][\omega^-\not{k}_3 f_{\mu\nu}] \\
&+[\omega^-\not{k}_1 f_{\mu\nu}][\omega^-\not{k}_3 f^{\mu\nu}]-[\omega^-\not{k}_2 f_{\mu\nu}][\omega^-\not{k}_3 f^{\mu\nu}]) \\
&+2D_{12}[\omega^-\not{k}_2 f_{\mu\nu}][\omega^-\not{k}_3 f^{\mu\nu}]+D_{11}[\omega^-\not{k}_3 f_{\mu\nu}][\omega^-\not{k}_3 f^{\mu\nu}]) \\
&+2D_{00}[\omega^+ f_{\mu\nu}\gamma_\alpha][\omega^- f^{\mu\nu}\gamma^\alpha]+D_{00}[\omega^- f_{\mu\nu}\gamma_\alpha][\omega^- f^{\mu\nu}\gamma^\alpha]].
\end{aligned}
\tag{3.54}
$$

In this long expression,

$$[w^{\pm}\not{k}_i f_{\mu\nu}] = (\bar{u}w^{\pm}\not{k}_i f_{\mu\nu}u)$$

α is the fine structure constant, $\omega^{\pm} = \frac{1\pm\gamma_5}{2}$, $f_{\mu\nu} = \gamma_\mu\gamma_\nu$ and $f^{\mu\nu} = \gamma^\mu\gamma^\nu$. Each tensor function is sandwiched with two Dirac chains consisting of $\omega^{\pm}$, gamma matrices and $\not{k}_i$. The reason why the Dirac spinnors are included in box graph is that most of the terms in the expression will cancel with each other without the Dirac spinors.

3.3 On-Shell Renormalization

The general idea of the renormalization scheme is to develop renormalization condition terms to remove the divergence of the amplitude. Additional renormalization conditions are introduced as calibrations to obtain the counter terms, which remove the divergence. The renormalized result of $\Sigma(k)$ is shown in the form of $\hat{\Sigma}(k)$.

On-shell renomalization conditions require the kinematic condition on-shell $k = m$ (for photon $m = 0$), where the pole of propagator occurs with a residue of 1. Therefore, we need to have the on-shell renomalization conditions as:

For photon-photon self energy,

1.

$$\hat{\Sigma}_{\gamma\gamma}(0) = 0; \tag{3.55}$$

2.

$$\left.\frac{\partial\hat{\Sigma}_{\gamma\gamma}}{\partial k^2}\right|_{k^2=0} = 0; \tag{3.56}$$

For fermion self energy,

3.

$$\lim_{\not{k}\to m}\frac{\hat{\Sigma}_{ff}(\not{k})}{\not{k}-m}u(k) = 0; \tag{3.57}$$

which leads to

$$\hat{\Sigma}_{ff}(\not{k} = m) = 0; \tag{3.58}$$

and using L'Hospital's rule,

$$\left.\frac{\partial\hat{\Sigma}_{ff}(\not{k})}{\partial\not{k}}\right|_{\not{k}=m} = 0 \tag{3.59}$$

The condition also includes the vertex Thomson limit as the non-relativistic charge:

4.

$$\left.\hat{\Gamma}^{\gamma_{ff}}_{\mu,tot}(q^2)\right|_{q^2=0} = -ieQ_f\gamma_\mu; \tag{3.60}$$

as well as the Ward-Takahashi identity:

5.

$$\left.\Gamma^{\gamma_{ff}}_{\mu}(q^2)\right|_{q^2=0} = -\left.\frac{\partial\Sigma_{ff}(\not{k})}{\partial k_\mu}\right|_{\not{k}=m}\cdot ieQ_f; \tag{3.61}$$

Note that the Ward-Takahashi identity is a mathematical identity derived from gauge symmetries.

There are several approaches to get the counter term for the on-shell renormalization condition. Most common ones are the multiplicative scheme and subtractive scheme. Both schemes introduce additional parameters, which will be solved using the on-shell renomalization conditions. As the names suggest, the parameters involved are different. These new parameters are used to construct counter terms.

3.3.1 Multiplicative Scheme

The multiplicative scheme or des Cloizeaux' scheme introduces scalar terms to re-size the parameters, fermion field ψ, electric charge e, mass m and boson field A_μ [6]. After re-scaling all of the parameters, the Lagrangian will be renormalized as a result.

Using $z_i = 1 + \delta z_i$ $(i = e, m, \psi, \gamma)$, the scaled terms can be written as

$$e_0 \to z_e e = (1 + \delta z_e)e;$$

$$m_0 \to z_m m = (1 + \delta z_m)m;$$

$$\psi_0 \to \sqrt{z_\psi}\psi \approx (1 + \frac{1}{2}\delta z_\psi)\psi;$$

and

$$A_\mu^0 \to \sqrt{z_\gamma} A_\mu \approx (1 + \frac{1}{2}\delta z;_\gamma) A_\mu$$

where $\delta z_\psi, \delta z_e, \delta z_m, \delta z_\gamma$ are undetermined constants.

Since the multiplicative scheme is a systematic approach, it applies to all the renormalizable fields. However, it may not be the most efficient approach. Therefore, this demonstration is only for QED at the one-loop level and no weak interactions are involved.

First of all, we need to obtain the renormalized Lagrangian term for the interaction of the fields. The original Lagrangian for QED is

$$L_{QED}^0 = \bar{\psi_0}(i\partial\!\!\!/ - e_0 A\!\!\!/_0 - m_0)\psi_0 - \frac{1}{4} F_{\mu\nu}^0 F_0^{\mu\nu}, \tag{3.62}$$

where $F_{\mu\nu} = \partial_\mu A_\nu - \partial_\nu A_\mu$. The renormalized Lagrangian for QED becomes

$$\begin{aligned}
\hat{L}_{QED} &= (1+\delta z_\psi)\bar{\psi}(i\partial\!\!\!/ - (1+\delta z_e)e\left(1+\frac{1}{2}\delta z_\gamma\right) A\!\!\!/ - (1+\delta z_m))\psi - \frac{1}{4}\left(1+\frac{1}{2}\delta z_\gamma\right)^2 F_{\mu\nu}F^{\mu\nu} \\
&= \bar{\psi}(i\partial\!\!\!/ - eA\!\!\!/ - m)\psi - \frac{1}{4}F_{\mu\nu}F_{\mu\nu} + \delta z_\psi \bar{\psi}(i\partial\!\!\!/ - eA\!\!\!/ - m)\psi + \bar{\psi}(-\delta z_e)eA\!\!\!/\psi + \\
&\quad + \bar{\psi}\left(-\frac{1}{2}\delta z_\gamma\right)eA\!\!\!/\psi + \bar{\psi}(-\delta z_m)m\psi - \frac{1}{4}F_{\mu\nu}F_{\mu\nu}\delta z_\gamma
\end{aligned} \tag{3.63}$$

The additional terms in $\hat{L}_{QED}$ are known as the counterterm Lagrangian from which we can derive the counterterms.

Vertex coupling:

$$\hat{\Gamma}_\mu = \Gamma_\mu + \delta\Gamma_\mu,$$

$$\delta\Gamma_\mu = -ieQ_f\gamma_\mu\left(\delta z_e + \frac{1}{2}\delta z_\gamma + \delta z_\psi\right). \tag{3.64}$$

Fermion self energy loop:

$$\hat{\Sigma}_{ff} = \Sigma_{ff} + \delta\Sigma_{ff},$$

$$\delta\Sigma_{ff} = \not{k}\delta z_\psi - m(\delta z_\psi + \delta z_m). \tag{3.65}$$

Boson self energy loop:

$$\hat{\Sigma}_{\gamma\gamma} = \Sigma_{\gamma\gamma} + \delta\Sigma_{\gamma\gamma},$$

$$\delta\Sigma_{\gamma\gamma} = -ig_{\mu\nu}k^2\delta z_\gamma. \tag{3.66}$$

The goal of renormalization is to solve the counterterms in order to obtain the renormalized amplitude. To do that, we need to solve all the scaling constants δz_i first.

Part 1: We start from the renormalization conditions of the boson self energy loop.

$$\hat{\Sigma}_{\gamma\gamma}(k^2) = \Sigma_{\gamma\gamma}(k^2) + k^2\delta z_\gamma \tag{3.67}$$

Since

$$\Sigma_{\gamma\gamma}(k^2) = k^2\Pi_{\gamma\gamma}(k^2)$$

hence

$$\hat{\Sigma}_{\gamma\gamma}(0) = k^2\Pi_{\gamma\gamma}(k^2) + k^2\delta z_\gamma = 0$$

Applying renormalization condition No. 2 from Eqn 3.56

$$\left.\frac{\partial\hat{\Sigma}_{\gamma\gamma}}{\partial k^2}\right|_{k^2=0} = \left(\frac{\partial\Sigma_{\gamma\gamma}}{\partial k^2} + \delta z_\gamma\right)_{k^2=0} = 0,$$

which gives

$$\delta z_\gamma = -\left.\frac{\partial\Sigma_{\gamma\gamma}}{\partial k^2}\right|_{k^2=0}. \tag{3.68}$$

Therefore,

$$\hat{\Sigma}_{\gamma\gamma}(k^2) = \Sigma_{\gamma\gamma}(k^2) - k^2\left.\frac{\partial\Sigma_{\gamma\gamma}}{\partial k^2}\right|_{k^2=0}.$$

Here, $\hat{\Sigma}^{\mu\nu}_{\gamma\gamma}$ represent the sum of γ γ self energy loop at one loop level and at higher orders (shaded), as shown in Figure 3.5.

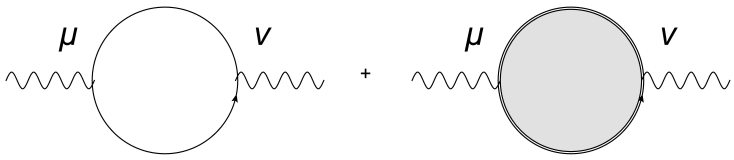

Figure 3.5: Feynman diagrams for $\hat{\Sigma}^{\mu\nu}_{\gamma\gamma}$.

Part 2: One can apply the vertex Thomson limit.

we have $\hat{\Gamma}^{\gamma_{ff}}_{\mu,tot}$ as the sum of all the Feynman diagrams for vertex, including tree level, one loop level and all the higher order ones.

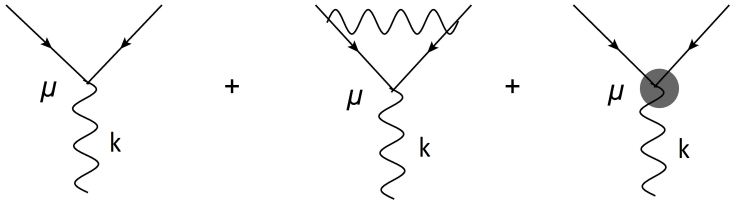

Figure 3.6: Feynman diagrams for $\hat{\Gamma}^{\gamma_{ff}}_{\mu,tot}$.

$$\hat{\Gamma}^{\gamma_{ff}}_{\mu,tot}(k^2) = -ieQ_f\gamma_\mu + ie\left[F_1(k^2)\gamma_\mu + \frac{1}{2m}\sigma_{\mu\alpha}k^\alpha F_2(k^2)\right]Q_f - ie\gamma_\mu\left(\delta z_e + \frac{1}{2}\delta z_\gamma + \delta z_\psi\right)Q_f.$$

Here, the middle term

$$ie\left[F_1(k^2)\gamma_\mu + \frac{1}{2m}\sigma_{\mu\alpha}k^\alpha F_2(k^2)\right]Q_f$$

represents the vertex at the one loop level, where $F_1(k^2)$ is the Dirac Form factor, $F_2(k^2)$ is the Pauli Form Factor and $\sigma_{\mu\alpha} = \frac{i}{2}[\gamma_\mu, \gamma_\alpha]$. Applying renormalization condition No. 4 (Eqn 3.60) ,

$$-ieQ_f\gamma_\mu = -ieQ_f\gamma_\mu + ie\left[F_1(0)\gamma_\mu + 0\right]Q_f - ie\gamma_\mu\left(\delta z_e + \frac{1}{2}\delta z_\gamma + \delta z_\psi\right)Q_f,$$

which leads to

$$\delta z_e + \frac{1}{2}\delta z_\gamma + \delta z_\psi = F_1(0), \tag{3.69}$$

$$\hat{\Sigma}_{ff}(\not{k}) = \not{k}\Sigma_v(k^2) + m\Sigma_s(k^2) + \not{k}\delta z_\psi - m(\delta z_\psi + \delta z_m).$$

Part 3: Using renormalization conditions on the fermion self energy loop: The first step of this part is to separate $\Sigma_{ff}(\not{k})$ into two parts:

$$\Sigma_{ff}(\not{k}) = \not{k}\Sigma_v(k^2) + m\Sigma_s(k^2).$$

Σ_v and Σ_s stand for the vectors part and the scalar part of Σ_{ff} respectively. The reason why we distinguished them from each other is that they need to be differentiated using different rules.

Using the renormalization condition from Eqn. 3.58

$$\hat{\Sigma}_{ff}(\not{k} = m) = 0,$$

Therefore,

$$\hat{\Sigma}_{ff}(\not{k} = m) = \not{k}\Sigma_v(m^2) + m\Sigma_s(m^2) + \not{k}\delta z_\psi - m(\delta z_\psi + \delta z_m) = 0, \tag{3.70}$$

which leads to

$$m\Sigma_v(m^2) + m\Sigma_s(m^2) + m\delta z_\psi - m\delta z_\psi - m\delta z_m = 0,$$

$$\delta z_m = \Sigma_v(m^2) + \Sigma_s(m^2). \tag{3.71}$$

The next step is to solve

$$\frac{\partial \Sigma_{ff}(\not{k})}{\partial k_\mu} = \frac{\partial k_\alpha \gamma^\alpha}{\partial k_\mu}\Sigma_v(k^2) + 2k_\mu \not{k}\frac{\partial \Sigma_v(k^2)}{\partial k^2} + 2mk_\mu \frac{\partial \Sigma_s}{\partial k^2}.$$

We used

$$\frac{\partial k_\alpha \gamma^\alpha}{\partial k_\mu} = g_{\alpha\mu}\gamma^\alpha = \gamma_\mu,$$

$$\left.\frac{\partial \Sigma_{ff}(\not{k})}{\partial k_\mu}\right|_{\not{k}=m} = \gamma_\mu \Sigma_v(m^2) + 2mk_\mu \left.\frac{\partial \Sigma_v(k^2)}{\partial k^2}\right|_{k^2=m^2} + 2mk_\mu \left.\frac{\partial \Sigma_s(k^2)}{\partial k^2}\right|_{k^2=m^2},$$

and when $\not{k} = m$,

$$mk_\mu = \not{k}k_\mu = \gamma^\alpha k_\alpha k_\mu = \gamma_\mu k_\alpha k^\alpha = m^2\gamma_\mu.$$

Therefore,

$$\left.\frac{\partial \Sigma_{ff}(\not{k})}{\partial k_\mu}\right|_{\not{k}=m} = \gamma_\mu \Sigma_v(m^2) + 2m^2\gamma_\mu \left.\frac{\partial \Sigma_v(k^2)}{\partial k^2}\right|_{k^2=m^2} + 2m^2\gamma_\mu \left.\frac{\partial \Sigma_s(k^2)}{\partial k^2}\right|_{k^2=m^2}. \tag{3.72}$$

The renormalization condition from Eqn. 3.59 is

$$\left.\frac{\partial \hat{\Sigma}_{ff}(\not{k})}{\partial \not{k}}\right|_{\not{k}=m} = 0.$$

Apply this condition to the Eqn. 3.72,

$$\left.\frac{\partial \hat{\Sigma}_{ff}(\not{k})}{\partial \not{k}}\right|_{\not{k}=m} = \Sigma_v(k^2) + 2m^2 \left.\frac{\partial \Sigma_v}{\partial k^2}\right|_{k^2=m^2} + 2m^2 \left.\frac{\partial \Sigma_s}{\partial k^2}\right|_{k^2=m^2} + \delta z_\psi = 0,$$

with the knowledge that

$$\left.\frac{\partial k^2}{\partial \not{k}}\not{k}\right|_{\not{k}=m} = 2m^2.$$

We can have

$$\delta z_\psi = -\Sigma_v(k^2) - 2m^2 \left.\frac{\partial \Sigma_v}{\partial k^2}\right|_{k^2=m^2} - 2m^2 \left.\frac{\partial \Sigma_s}{\partial k^2}\right|_{k^2=m^2}. \tag{3.73}$$

Part 4: Now we apply the Ward-Takahashi identity.

One can multiply ieQ_f with Eqn. 3.72 to get the right-hand side of the Ward-Takahashi identity and the left-hand side was shown in part 2. Now applying the

Ward-Takahashi identity, we have

$$\begin{aligned}\Gamma^{\gamma ff}_{\mu}\Big|_{k^2=0} &= ieQ_f\gamma_\mu F_1(0) = -\left.\frac{\partial\Sigma_{ff}(\not{k})}{\partial k_\mu}\right|_{\not{k}=m}\cdot ieQ_f \\ &= -\gamma_\mu ieQ_f\left[\Sigma_v(m^2)+2m^2\left(\frac{\partial\Sigma_v}{\partial k^2}+\frac{\partial\Sigma_s}{\partial k^2}\right)_{k^2=m^2}\right],\end{aligned} \tag{3.74}$$

which leads to

$$F_1(0) = -\Sigma_v(m^2)+2m^2\left(\frac{\partial\Sigma_v}{\partial k^2}-\frac{\partial\Sigma_s}{\partial k^2}\right)_{k^2=m^2}, \tag{3.75}$$

$$\delta z_e+\frac{1}{2}\delta z_\gamma+\delta z_\psi = -\Sigma_v(m^2)-2m^2\left(\frac{\partial\Sigma_v}{\partial k^2}+\frac{\partial\Sigma_s}{\partial k^2}\right)_{k^2=m^2}. \tag{3.76}$$

with from Eqn. 3.73 and 3.68,

$$\delta z_\psi = -\left(\Sigma_v(m^2)+2m^2\left.\frac{\partial\Sigma_v}{\partial k^2}\right|_{k^2=m^2}+2m^2\left.\frac{\partial\Sigma_s}{\partial k^2}\right|_{k^2=m^2}\right),$$

$$\delta z_\gamma = -\left.\frac{\partial\Sigma_{\gamma\gamma}}{\partial k^2}\right|_{k^2=0}.$$

we can solve for δz_e as

$$\delta z_e = -\frac{1}{2}\delta z_\gamma = \frac{1}{2}\left.\frac{\partial\Sigma_{ff}}{\partial k^2}\right|_{k^2=0}. \tag{3.77}$$

So far we have solved all four scaling constants δz_e, δz_m, δz_γ and δz_ψ as shown in Eqn. 3.77, 3.71, 3.68 and 3.73. Now the renormalized graphs with the corresponding counterterms are

Vertex:

$$\hat{\Gamma}_\mu(q^2) = \Gamma_\mu(q^2)-ie\gamma_\mu Q_f F_1(0) = \Gamma_\mu(q^2)-\Gamma_\mu(0), \tag{3.78}$$

Boson self energy loop:

$$\begin{aligned}\hat{\Sigma}_{\gamma\gamma} &= \Sigma_{\gamma\gamma} + \delta\Sigma_{\gamma\gamma} \\ &= \Sigma_{\gamma\gamma} - ig_{\mu\nu}k^2\delta z_\gamma \\ &= \Sigma_{\gamma\gamma} - ig_{\mu\nu}k^2 - \left.\frac{\partial\Sigma_{\gamma\gamma}}{\partial k^2}\right|_{k^2=0};\end{aligned} \tag{3.79}$$

Fermion self energy loop:

$$\begin{aligned}\hat{\Sigma}_{ff}(\not{k}) &= \Sigma_{ff}(\not{k}) + \not{k}\delta z_\psi - m(\delta z_\psi + \delta z_m) \\ &= \Sigma_{ff}(\not{k}) - \not{k}\left.\frac{\partial\Sigma_{ff}(\not{k}}{\partial\not{k}}\right|_{\not{k}=m} - m\left(-\left.\frac{\partial\Sigma_{ff}(\not{k})}{\partial\not{k}}\right|_{\not{k}=m} + \Sigma_v(m^2) + \Sigma_s(m^2)\right) \\ &= \Sigma_{ff}(\not{k}) - \left.\frac{\partial\Sigma_{ff}(\not{k})}{\partial\not{k}}(\not{k}-m)\right|_{\not{k}-m} - \underbrace{m\left[\Sigma_v(m^2) + \Sigma_s m^2\right]}_{\Sigma_{ff}(\not{k})|_{\not{k}=m}} \\ &= \Sigma_{ff}(\not{k}) - \left.\frac{\partial\Sigma_{ff}(\not{k})}{\partial\not{k}}(\not{k}=m)\right|_{\not{k}=m} - \Sigma_{ff}(\not{k})|_{\not{k}=m}\,.\end{aligned} \tag{3.80}$$

3.3.2 Subtractive Scheme

The subtractive scheme is not a published method. However, it has been mathematically proven [19]. In many occasions, the subtractive scheme is easier to implement. A divergence exists in the vector boson self energy loops and is in the form of

$$\Sigma(k^2) = \Sigma_{fin}(k^2) + \Sigma_\Delta(k^2), \tag{3.81}$$

where

$$\Sigma_\Delta(k^2) = (a + bk^2)\Delta.$$

Here a, b are constants and $\frac{2}{\epsilon} = \Delta$ is divergent.

In order to obtain the non-divergent expression for the truncated self energy graph

$\hat{\Sigma}(k^2)$, we remove the divergences by subtraction.

$$\hat{\Sigma}(k^2) = \Sigma(k^2) - \Sigma(\Lambda_0) - \left.\frac{\partial\Sigma(k^2)}{\partial k^2}\right|_{k^2=\Lambda_1^2},$$

$$\begin{aligned}
\hat{\Sigma}(k^2) &= \Sigma_{fin}(k^2) - \Sigma_{fin}(\Lambda_0^2) - \left.\frac{\partial\Sigma_{fin}(k^2)}{\partial k^2}\right|_{k^2=\Lambda_1^2} + (a+bk^2)\Delta - (a+b\Lambda_0^2)\Delta - b\Delta(k^2-\Lambda_0^2) \\
&= \Sigma_{fin}(k^2) - \Sigma_{fin}(\Lambda_0^2) - \left.\frac{\partial\Sigma_{fin}(k^2)}{\partial k^2}\right|_{k^2=\Lambda_1^2} + a\Delta + bk^2\Delta - a\Delta - a\Lambda_0^2\Delta - b\Delta k^2 + b\Delta\Lambda_0^2 \\
&= \Sigma_{fin}(k^2) - \Sigma_{fin}(\Lambda_0^2) - \left.\frac{\partial\Sigma_{fin}(k^2)}{\partial k^2}\right|_{k^2=\Lambda_1^2}.
\end{aligned} \tag{3.82}$$

Therefore, the final expression for $\hat{\Sigma}(k^2)$ is

$$\hat{\Sigma}(k^2) = \Sigma_{fin}(k^2) - \Sigma_{fin}(\Lambda_0) - \left.\frac{\partial\Sigma_{fin}(k^2)}{\partial k^2}\right|_{k^2=\Lambda_1^2}, \tag{3.83}$$

which is convergent, as long as valid $\Lambda_{0,1}$ are provided.

The subtractive scheme is more straight forward and effective. The general idea is to find certain energy levels/momenta (Λ) where Feynman graph themselves become counterterms.

Now we apply the subtractive scheme to QED. The divergence of the Feynman graphs can be written as:

1.

$$\Sigma_\Delta^{\gamma\gamma}(k^2) = (a_1 + b_1k^2)\Delta, \quad \Delta = \frac{2}{4-D};$$

2.

$$\Sigma_\Delta^{ff}(\not{k}) = (a_2 + b_2\not{k})\Delta;$$

3.

$$\Gamma^{\Delta}_{\mu}(k^2) = c\Delta ie\gamma_{\mu}.$$

Now, introduce the set of scales, Λ.

Part 1: For a boson self energy graph, we have the expression:

$$\hat{\Sigma}_{\gamma\gamma}(k^2) = \Sigma_{\gamma\gamma}(k^2) - \Sigma_{\gamma\gamma}(\Lambda_0^2) - \left.\frac{\partial\Sigma_{\gamma\gamma}}{\partial k^2}\right|_{k^2=\Lambda_1^2}(k^2 - \Lambda_0^2), \tag{3.84}$$

e.g.

$$\hat{\Sigma}^{div}_{\gamma\gamma} = (a_1 + b_1k^2)\Delta - (a_1 + b_1\Lambda_0^2)\Delta - b_1\Delta(k^2 - \Lambda_0^2) = 0.$$

Conditions:

a)

$$\left.\frac{\partial\hat{\Sigma}_{\gamma\gamma}(k^2)}{\partial k^2}\right|_{k^2=0} = 0;$$

b)

$$\hat{\Sigma}_{\gamma\gamma}(0) = 0;$$

which leads to

a)

$$\left.\frac{\partial\Sigma_{\gamma\gamma}}{\partial k^2}\right|_{k^2=0} - \left.\frac{\partial\Sigma_{\gamma\gamma}}{\partial k^2}\right|_{k^2=\Lambda_1^2} = 0,$$

$$\Lambda_0 = \Lambda_1 = 0;$$

b)

$$\Sigma_{\gamma\gamma}(0) - \Sigma_{\gamma\gamma}(\Lambda_0^2) - \left.\frac{\partial\Sigma_{\gamma\gamma}}{\partial k^2}\right|_{k^2=\Lambda_1^2}(-\Lambda_0^2) = 0,$$

$$\Lambda_1 = \Lambda_0;$$

Part 2: For a truncated fermion self energy graph, the expression is:

$$\hat{\Sigma}_{ff}(\not{k}) = \Sigma_{ff}(\not{k}) - \Sigma_{ff}(\not{k})|_{\not{k}=\Lambda_3} - \left.\frac{\partial \Sigma_{ff}}{\partial \not{k}}\right|_{\not{k}=\Lambda_4} (\not{k} - \Lambda_3).$$

Using the renormalization conditions

$$\frac{\partial \hat{\Sigma}_{ff}}{\partial \not{k} - m} u(\not{k}) = 0,$$

$$\Sigma_{ff}(\not{k} = m) = 0,$$

$$\left.\frac{\partial \Sigma_{ff}}{\partial \not{k}}\right|_{\not{k}=m} = 0;$$

c)

$$\Sigma_{ff}(0) - \Sigma_{ff}(\Lambda_3) - \left.\frac{\partial \Sigma_{ff}}{\partial \not{k}}\right|_{\not{k}=\Lambda_4} (m - \Lambda_3) = 0,$$

which leads to

$$\Lambda_3 = m;$$

d)

$$\left.\frac{\partial \Sigma_{ff}}{\partial \not{k}}\right|_{\not{k}=m} - \left.\frac{\partial \Sigma_{ff}}{\partial \not{k}}\right|_{\not{k}=\Lambda_4} = 0,$$

$$\Lambda_4 = m;$$

Part 3: Now apply the same process for a vertex:

$$\hat{\Gamma}^{\mu}(k^2) = \Gamma^{\mu}(k^2) - \Gamma^{\mu}(\Lambda_5^2),$$

$$\hat{\Gamma}^{\mu}_{ff}(k^2 = 0) = ieQ_f\gamma^{\mu} = ieQ_f\gamma^{\mu} + \Gamma^{\mu}(k^2) - \Gamma^{\mu}(\Lambda_5^2);$$

which provides the result of

$$\Lambda_5^2 = 0.$$

As the derivation demonstrates, the subtractive scheme, at the QED level, is a much easier and straight forward method. It provides the exact same counterterms as the multiplicative scheme.

Chapter 4

Computation and Analysis

4.1 Scattering Channel

The chosen scattering channel is electron-electron scattering, known as Möller scattering ($ee \to ee$) and its antimatter version- positron-positron scattering.

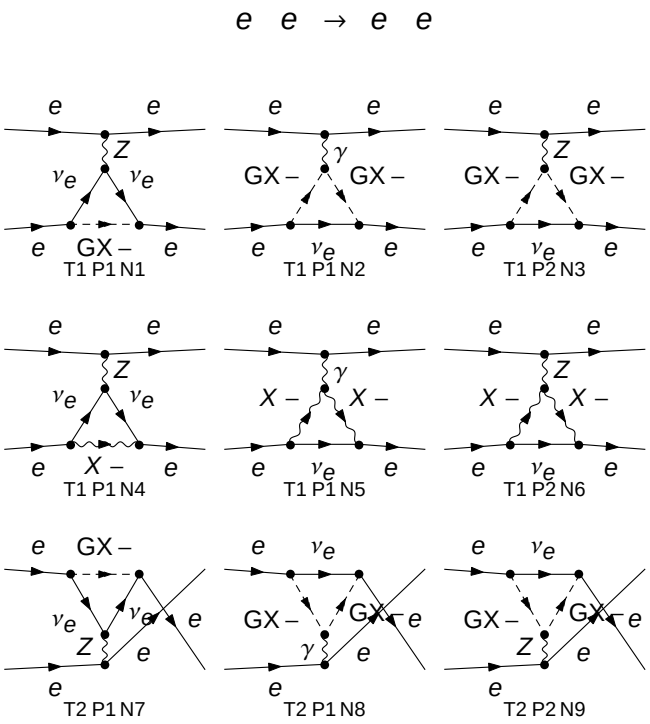

Figure 4.1: Feynman diagrams for triangle graphs.

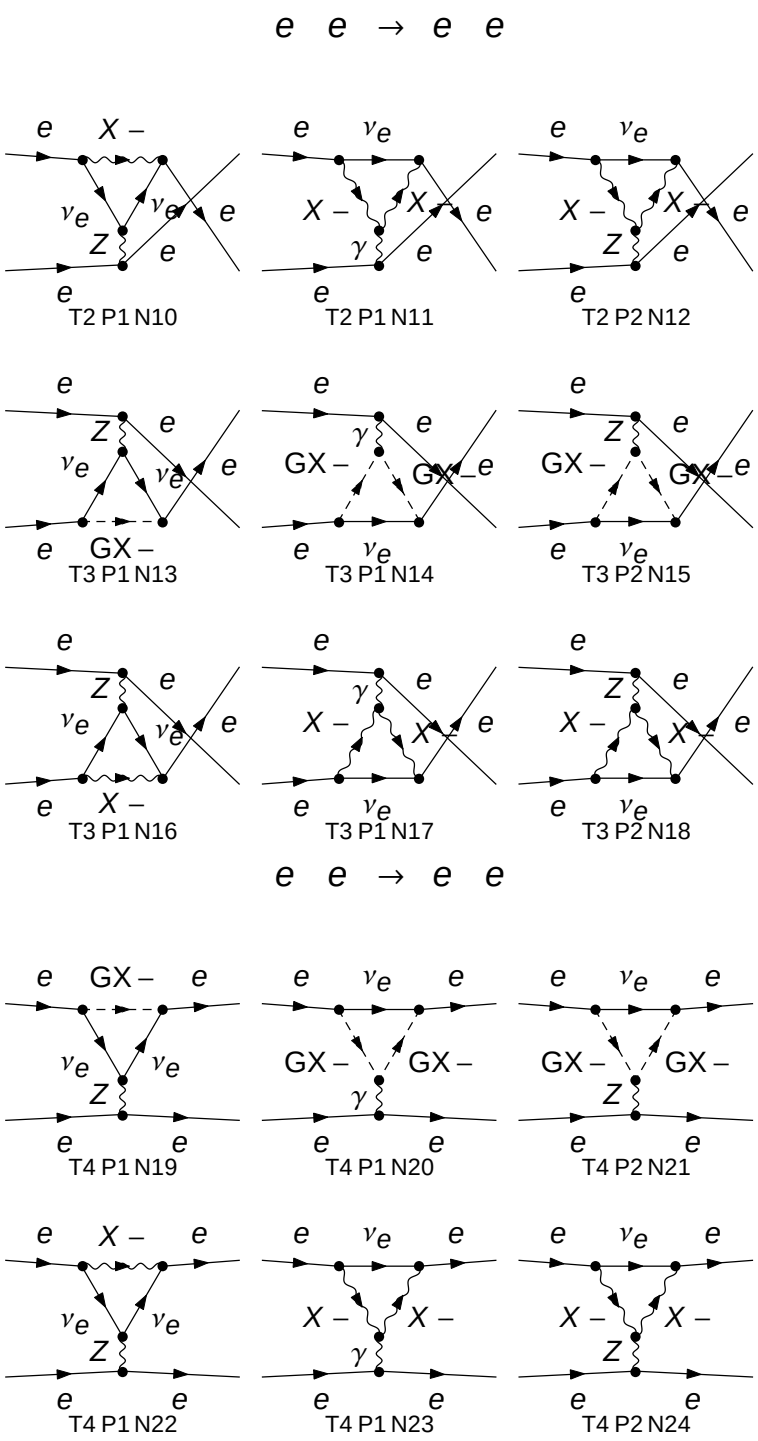

Figure 4.2: Cont. Feynman diagrams for triangle graphs.

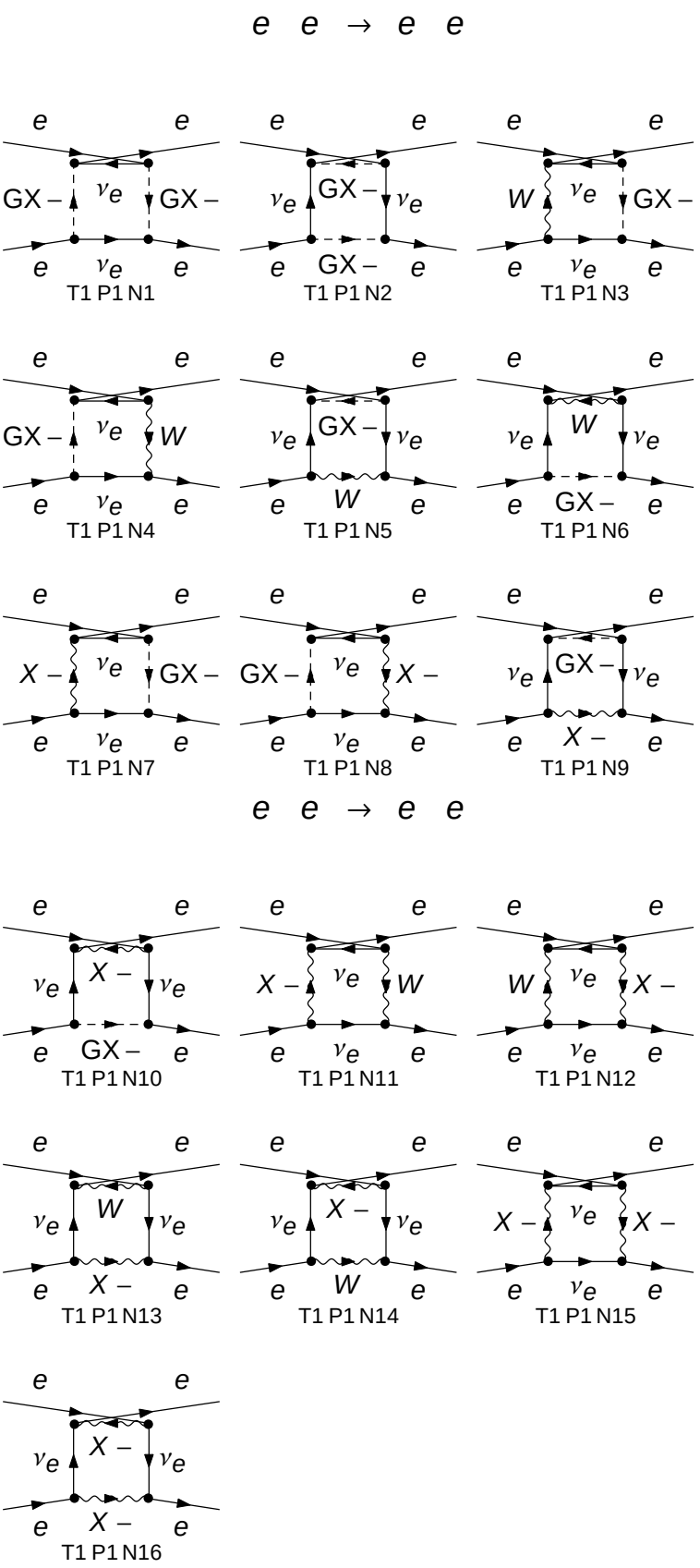

Figure 4.3: Feynman diagrams for box graphs.

There are only box graphs and triangle graphs, which makes the calculations less difficult. Self energy graphs did not appear because $X^{\pm}$ are charged particles, thus they cannot appear individually in a neutral current. If they both appear inside of the loop, there would not be any difference between electron-electron scattering and positron-positron scattering to generate CP violation.

Note that there are additional particles GX^+ and GX^- involved. They are the ghost field particle for X^+ and X^- respectively.

4.2 Asymmetry

In order to test the impact of the new $X^{\pm}$ particles on strong CP violation, we have to run a series of calculations for X^- in electron-electron scattering and X^+ in positron-positron scattering and compare the difference. A new physical measurable is introduced to better display the impact,

$$A_{\pm} = \frac{\sigma_+ - \sigma_-}{\sigma_+ + \sigma_-}. \tag{4.1}$$

In Eqn. 4.1, σ_+ is the cross section of positron scattering with X^+, and σ_- is the cross section of electron scattering with X^-. Note that both of the cross sections contain all the SM Feynman diagram contribution up to the one loop level. Therefore, we can divide the cross section of positron scattering and electron scattering in this manner:

$$\sigma_+ = |A_1 + A_2 + A_3 + \cdots|^2 = |A_{tree} + A_{loop} + A_{X^+}|^2, \tag{4.2}$$

$$\sigma_- = |B_1 + B_2 + B_3 + \cdots|^2 = |B_{tree} + B_{loop} + B_{X^-}|^2, \tag{4.3}$$

where A_i is the corresponding amplitude from the ith diagram in positron scattering

and B_i is the corresponding amplitude from the ith diagram in electron scattering. A_{X^+} and B_{X^-} are the sum of the amplitudes of the Feynman diagrams involving X^+ and X^- respectively. Similarly, A_{tree} and A_{loop} are the sum of the amplitudes for tree level contribution and one loop level SM contribution respectively. Eqn. 4.1 then becomes:

$$A_{\pm} = \frac{|A_{tree} + A_{loop} + A_{X^+}|^2 - |B_{tree} + B_{loop} + B_{X^-}|^2}{|A_{tree} + A_{loop} + A_{X^+}|^2 + |B_{tree} + B_{loop} + B_{X^-}|^2}, \tag{4.4}$$

with $A_{tree} = B_{tree}$ and $A_{loop} = B_{loop}$.

$$A_{\pm} = \frac{|A_{X^+}|^2 + 2Re(A_{tree}A^*_{X^+})2 - |B_{X^-}|^2 - 2Re(B_{tree}B^*_{X^-})}{2|A_{tree}|^2}. \tag{4.5}$$

Without an introduced CP violating phase, the amplitudes of electron scattering and positron scattering are conjugates of each other; therefore, they have the same cross section, which produces no CP violation, $A_{tree} = B_{tree}$. There are also one loop level Feynman diagrams without $X^{\pm}$. For the same reason, their contributions (A_{loop} and B_{loop}) cancel out in the numerator as well. In addition, $|A_{X^+}|^2$ and $|B_{X^-}|^2$ are the second order terms, which can also be dropped from the numerator. A_{loop}, B_{loop}, A_{X^+} and B_{X^-} are insignificant terms compared to A_{tree} and B_{tree}, which can be dropped from the denominator, which leaves the leading term in the denominator as $2|A_{tree}|^2$. Then the asymmetry becomes:

$$A_{\pm} = \frac{Re(A_{tree}A^*_{X^+}) - Re(A_{tree}B^*_{X^-})}{|A_{tree}|^2}. \tag{4.6}$$

The tree contributions and the one loop SM contributions are all canceled. The most dominant term in the numerator of Eqn. 4.6 is directly proportional to A_{X^+} and B_{X^-}, and hence is the most sensitive observable to the new physics particles.

4.3 Mathematica

All the calculations were performed in Mathematica. There are four main packages used in the notebook – FeynArts, FormCalc, Form and LoopTools [20][36]. FeynArts generates Feynman diagrams for the corresponding interaction. FormCalc and Form perform similarly, as they both calculate tree level and one loop level graphs with renormalization implemented. At the end of the calculation, LoopTools takes the final expression of all the graphs and finishes the numerical integration.

To introduce the $X^{\pm}$ model in the calculation, I expanded both the FeynArts and FormCalc model files. In FeynArts, $X^{\pm}$ and all the coupling of any new interactions with them were registered. In FormCalc, model file was modified to implemented the renormalization scheme for $X^{\pm}$ interactions. Thanks to the direct mathematical connection between the $X^{\pm}$ model to the SM, this modification is straightforward.

There are two model files responsible for FeynArts to generate the topology of the Feynman diagram and the corresponding amplitude, namely the class model file (mod) file and generic model file (gen) file. Mod file contains the definition of a classes model for FeynArts, "All particles of a model are arranged in classes. A class is conceptually similar, but not identical, to a multiplet[20]". The .gen file contains generic analytical propagators and couplings. Both files are required to generate Feynman diagram and amplitude, since they are essentially a collection of row (.gen) and column (.mod) matrices. Also due to this nature, the order of the entries for the same coupling on both files need to match.

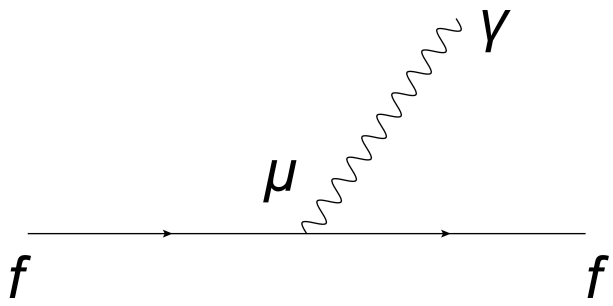

Figure 4.4: Feynman diagram for a fermion-fermion-photon vertex with index μ.

For example, at the QED level, a fermion-fermion-photon vertex, shown as Figure 4.4, can be programmed using the .gen and .mod file

$$\begin{aligned}\Gamma_\mu &= ieQ_f\gamma_\mu = ie\left[g_R\gamma_\mu w_+ + g_L\gamma_\mu w_-\right] \\ &= \underbrace{[\gamma_\mu w_+, \gamma_\mu w_-]}_{.gen} \underbrace{\begin{bmatrix} ieg_R \\ \\ ieg_L \end{bmatrix}}_{.mod}.\end{aligned} \tag{4.7}$$

Here $w_\pm = \frac{1\pm\gamma_5}{2}$ and $g_L = g_R = Q_f$.

In the mod file, two new physics particles, X^- and X^+, were introduced as X[1] and X[2], as well as their gauge-fixing ghost partners GX^- and GX^+. The programmed couplings involve $X^\pm$ and the electron, positron, electron neutrino, photon and Z boson. For example, for a fermion-fermion-$X^\pm$ coupling, the code in the mod file is

```
(* F-F-X: *)
 C[ -F[1, {j1}], F[2, {j2}], -X[1] ] ==
    IndexDelta[j1, j2] *I EL/(Sqrt[2] SW) *
 { {a1^2*PHAS1 + a2^2*PHAS2, 0},
     { a1^2*PHAS1 + a2^2*PHAS2, 0}},
```

```
 C[ F[1, {j1}], -F[2, {j2}], X[1] ] ==
  IndexDelta[j1, j2]  *I EL/(Sqrt[2] SW) *
{ {epsc1^2*Conjugate[PHAS1] + a2^2*Conjugate[PHAS2], 0},
    {a1^2*Conjugate[PHAS1] + a2^2*Conjugate[PHAS2], 0}},


C[ -F[1, {j1}], F[2, {j2}], X[2] ] ==
   IndexDelta[j1, j2]  *I EL/(Sqrt[2] SW) *
{ {a1^2*PHAS3 + a2^2*PHAS4, 0},
    { a1^2*PHAS3 + a2^2*PHAS4, 0}},

 C[ F[1, {j1}], -F[2, {j2}], -X[2] ] ==
  IndexDelta[j1, j2]  *I EL/(Sqrt[2] SW) *
{ {a1^2*Conjugate[PHAS3] + a2^2*Conjugate[PHAS4], 0},
    {a1^2*Conjugate[PHAS3] + a2^2*Conjugate[PHAS4], 0}},
```

where EL refers to electron charge, CW and SW represent $\cos\theta_W$ and $\sin\theta_W$. θ_W is the Weinberg angle. Note that all the lines in the mod file belong to a single class F-F-X and the corresponding generic coupling for such class was

```
 AnalyticalCoupling[ s1 F[j1, mom1], s2 F[j2, mom2],
     s3 X[j3, mom3, {li3}] ] ==
   G[-1][s1 F[j1], s2 F[j2], s3 X[j3]] .
  {  NonCommutative[DiracMatrix[li3], ChiralityProjector[-1]],
       NonCommutative[DiracMatrix[li3], ChiralityProjector[+1]] },
```

where DiracMatrix[li3] refers to γ^{li3} and ChiralityProjector[$\pm$1] refers to $\omega_{\pm}$.

Similarly, for a Z boson (V[2])/photon(V[1]) and $X^{\pm}$ coupling, the code in the mod file was

```
(* X-X-V:  *)
  C[ V[1], -X[1], X[1] ] == I EL *
    { {(a1^2*PHAS1 + a2^2*PHAS2)^2, 0} },

  C[ V[2], -X[1], X[1] ] == -I EL CW/SW *
    { {(a1^2*PHAS1 + a2^2*PHAS2)^2, 0} },

  C[ V[1], -X[2], X[2] ] == -I EL *
    { {(a1^2*PHAS3 + a2^2*PHAS4)^2, 0} },

  C[ V[2], -X[2], X[2] ] == I EL CW/SW *
    { {(a1^2*PHAS3 + a2^2*PHAS4)^2, 0} },
```

and the X-X-V class was

```
  AnalyticalCoupling[ s1 V[j1, mom1, {li1}], s2 X[j2, mom2, {li2}],
      s3 X[j3, mom3, {li3}] ] ==
    G[-1][s1 V[j1], s2 X[j2], s3 X[j3]] .
      { MetricTensor[li1, li2] FourVector[mom2 - mom1, li3] +
          MetricTensor[li2, li3] FourVector[mom3 - mom2, li1] +
          MetricTensor[li3, li1] FourVector[mom1 - mom3, li2] },
```

where MetricTensor[li1, li2] is $g^{li1,li2}$ and FourVector refers to four momentum. The propagators for $X^{\pm}$ were written as

```
  AnalyticalPropagator[External][ s1 X[j1, mom, {li2}] ] ==
    PolarizationVector[X[j1], mom, li2],

  AnalyticalPropagator[Internal][ s1 X[j1, mom, {li1} -> {li2}] ] ==
    -I PropagatorDenominator[mom, Mass[X[j1]]] *
    (MetricTensor[li1, li2] - (1 - GaugeXi[X[j1]]) *
```

```
FourVector[mom, li1] FourVector[mom, li2] *
PropagatorDenominator[mom, Sqrt[GaugeXi[X[j1]]] Mass[X[j1]]],
```

where the external propagator is the plane wave solution to the X field and the internal propagator is the one derived in Chapter 2. All the other couplings are programmed in the same fashion. Once they are implemented and loaded in the Mathematica notebook, one can generate all the Feynman diagrams and their amplitudes. There was no self energy graphs involved due to charge conservation and the CP violation requirement; box graphs do not diverge and triangle graphs use basic standard model subtraction schemes. FormCalc was modified to perform the subtractive scheme of the vertex at zero momentum transfer. The subtractive scheme is introduced in the Chapter 3 in detail. The FormCalc model file used in the calculation is not significantly different from the SM one, other than the fact that new particles are registered.

After obtaining the desired Feynman diagrams and amplitudes, the rest of the notebook is straight forward: squaring the amplitude and inputting all the information/constants, such as helicity, scattering angle, total energy, masses for all the involved particles. LoopTools is also involved to calculate all the integrals. The expression of asymmetry was generated at the end the notebook. There are some parameters set in the notebook to test the divergence from FormCalc and the numerical stability of LoopTools. Note that the asymmetry will only depend on the coupling parameters a_1^2, a_2^2, the masses of $X^{\pm}$ and four phase factors.

The full Mathematica notebook is attached in the appendix.

4.4 Phase Factors

As demonstrated in the Mathematica section, the expression for asymmetry had been generated from the notebook with eight unknown parameters-the masses of the new particles, two coupling constants a_1, a_2, and four phase factors. Note that, for all the calculations, the energy is at 11 GeV, which matches the energy at Thomas Jefferson

National Accelerator Facility [5]. The scattering angle is 90 degrees. Plots are made to show the correlation between the asymmetry and these variables.

For all the figures in this section, the set parameters are $a_1 = 0.1$, and $a_2 = 0.2$.

The couplings are of the form

$$a_1^2 e^{i\delta_1 \pm i\phi_1} + a_2^2 e^{i\delta_2 \pm i\phi_2},$$

which makes the asymmetry a 5D sinusoidal function. In order to visualize it, all the plots of phase factors contains two varying parameters (δ_1 and ϕ_1) with (δ_2 and ϕ_2) depending on them. 3D plots with periodical patterns can be can be confusing and misleading without the rotation function. Therefore only one 3D plot is included. In the other plots, known as exclusion plots, the information of a 3D plot is shown in a 2D fashion. Exclusion plots are contour plots of those 3D plots with the exclusion of $A_\pm > 0$ the strong CP violation. The reason why I included the exclusion is that physically the sign of asymmetry should be either constantly positive or constantly negative. Based on the mathematical nature of the implanted phase factors, either sign of the asymmetry can produce the same maximum magnitude.

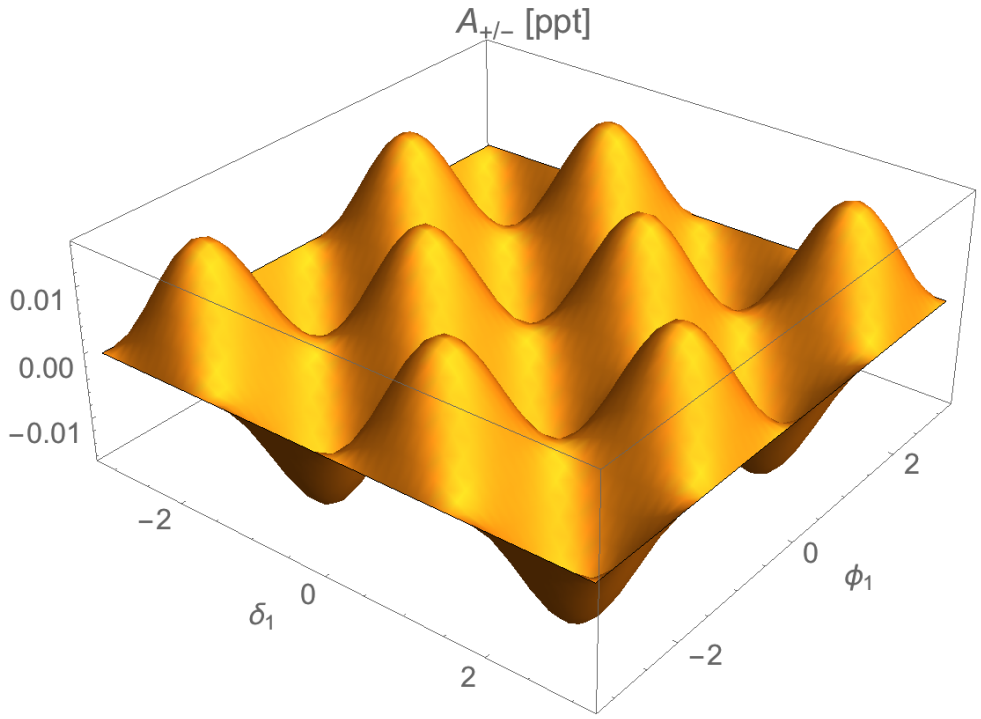

Figure 4.5: 3D plot for asymmetry in parts per trillion (ppt) vs δ_1 and ϕ_1 with $a_1 = 0.1$, $a_2 = 0.2$, $m_X = 50$ GeV, $\delta_2 = \delta_1$ and $\phi_2 = \phi_1$.

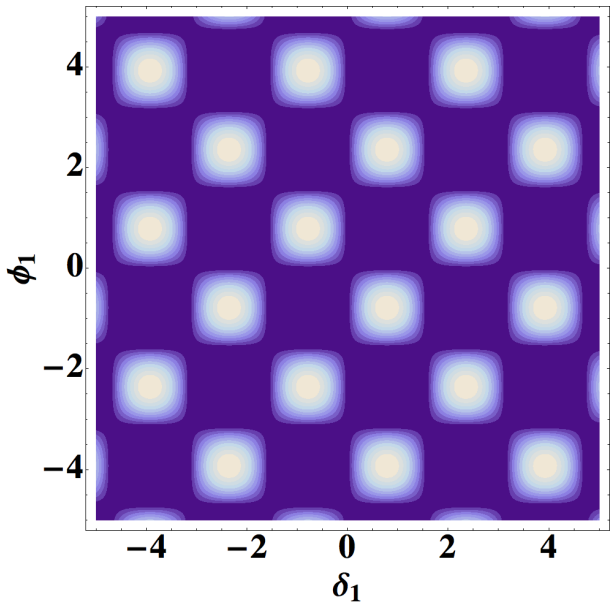

Figure 4.6: Exclusion plot with $a_1 = 0.1$, $a_2 = 0.2$, $m_X = 80$ GeV, $\delta_2 = \delta_1$ and $\phi_2 = \phi_1$.

In Figure 4.5, the plot presents as a sinusoidal wave. In the exclusion plot, the

white color indicates the minimum asymmetry and dark blue color indicates the excluded region ($A_{\pm} \geq 0$). Both the 3D plot and the exclusion plot show the same pattern of how the asymmetry changes with phase factors.

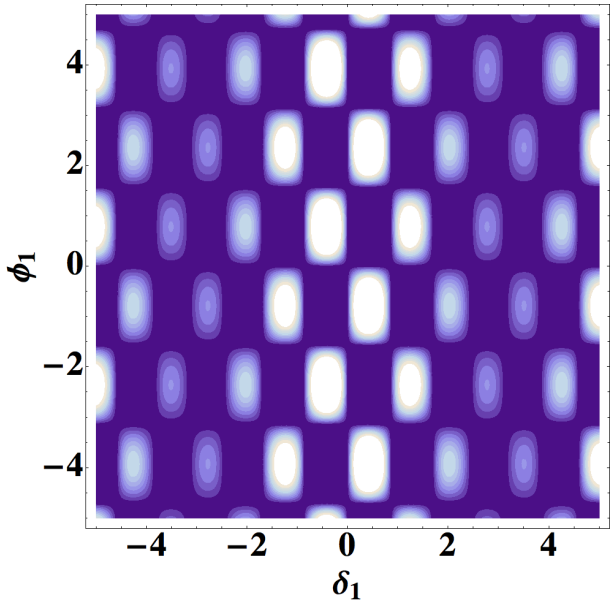

Figure 4.7: Exclusion plot with $a_1 = 0.1$, $a_2 = 0.2$, $m_X = 80$ GeV, $\delta_2 = 2\delta_1$ and $\phi_2 = \phi_1$.

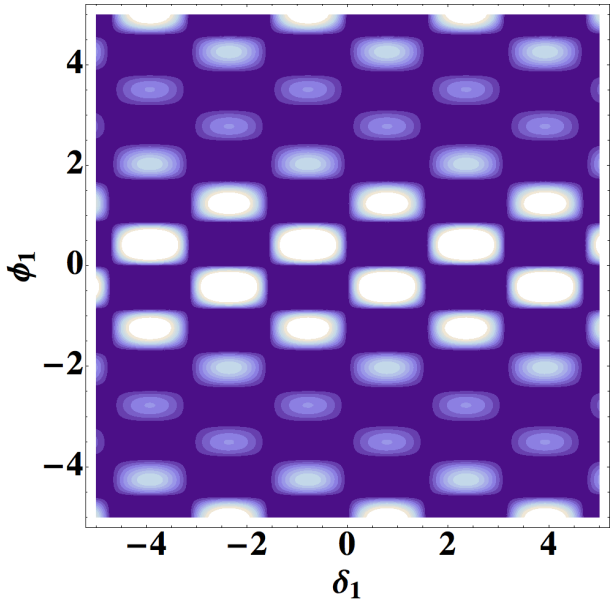

Figure 4.8: Exclusion plot with $a_1 = 0.1$, $a_2 = 0.2$, $m_X = 80$ GeV, $\delta_2 = \delta_1$ and $\phi_2 = 2\phi_1$.

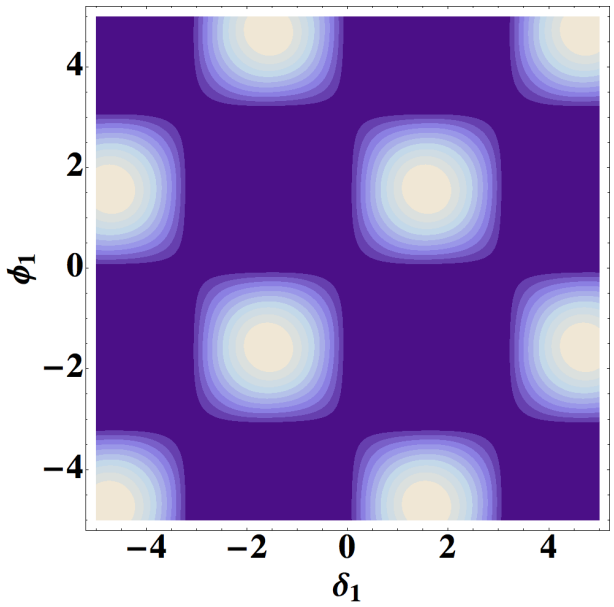

Figure 4.9: Exclusion plot with $a_1 = 0.1$, $a_2 = 0.2$, $m_X = 80$ GeV, $\delta_2 = 2\delta_1$ and $\phi_2 = 2\phi_1$.

The frequency of δ_1 and ϕ_1 can be different with asymmetric relationships between δ_1 and δ_2 and ϕ_1 and ϕ_2, as shown in Figure 4.7 and 4.8. With symmetric correlations, the periodic pattern only exists along the diagonal of the exclusion plots and its frequency depends on the scale of the the correlations, as demonstrated in Figure 4.9. Non-linear relationships affect the frequency of the pattern non-linearly.

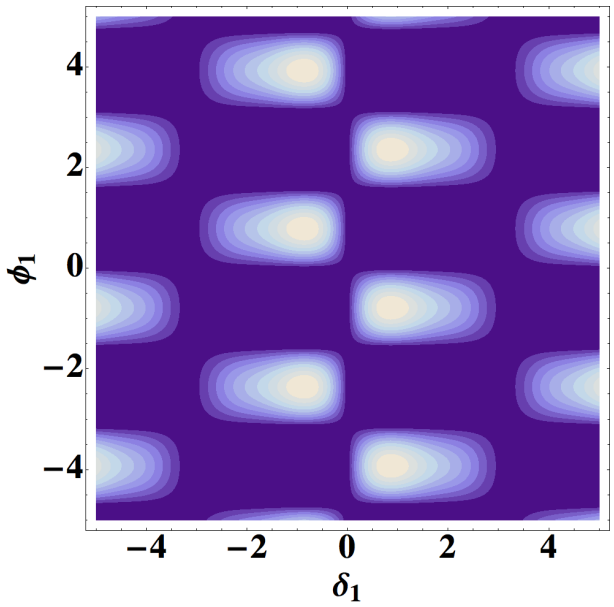

Figure 4.10: Exclusion plot with $a_1 = 0.1$, $a_2 = 0.2$, $m_X = 80$ GeV, $\delta_2 = \sin(\delta_1)$ and $\phi_2 = \phi_1$.

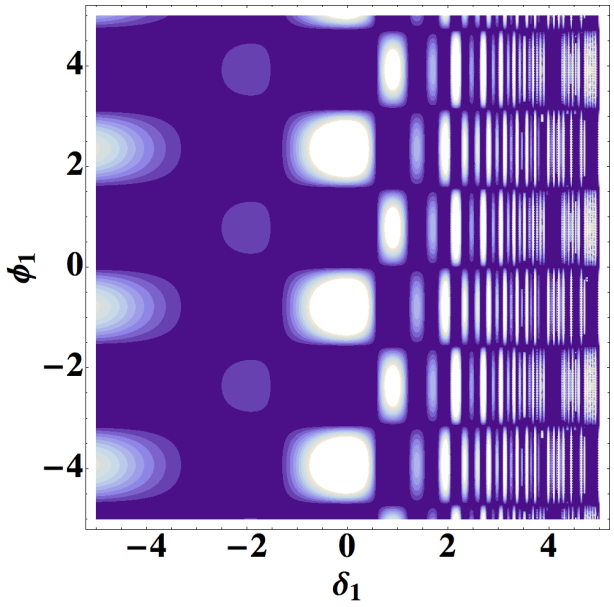

Figure 4.11: Exclusion plot with $a_1 = 0.1$, $a_2 = 0.2$, $m_X = 80$ GeV, $\delta_2 = \exp(\delta_1)$ and $\phi_2 = \phi_1$.

Note that the unstable pattern in Figure 4.11 is caused by Mathematica's memory limitation. With more plot points allowed, the inconsistency would disappear.

Overall, the phase factors indicate the $X^{\pm}$ model functions well in terms of computational results. In order to identify the theoretical cause for strong CP violation, the phase difference is vital. Not only do we need the magnitude to potentially observe the CP violation experimentally, but also need to identify the cause of such a violation mathematically. The phase factors provide a possible approach to locate the cause of strong CP violation. However, it would be challenging to measure the phase factors experimentally. Since each $X^{\pm}$ particles consists of two new physics loops, the contribution of the phase parameters are at two loop level instead of one loop level. We can expand the implication of $X^{\pm}$ to more channels, such as hadronic ones, which could help to measure the phase factors through high energy experiments as well.

4.5 Asymmetry Magnitude

From Eqn. 4.6, the asymmetry can be written as

$$A_{\pm} = \frac{Re(A_{tree}A^*_{X^+}) - Re(A_{tree}B^*_{X^-})}{|A_{tree}|^2}$$

By changing the phase factors, it is possible to find certain phases so that the asymmetry reaches the maximum magnitude. To solve it, we let $\delta_1 = \delta_2$ and $\phi_1 = \phi_2$. Then, we can treat $A^*_{X^-}$ as a polynomial function of $\left(e^{i\xi_1}\right)^2$ and $\left(e^{i\xi_1}\right)^4$, where

$$\delta_1 + \phi_1 = \delta_2 + \phi_2 = \xi_1$$

The order 2 and 4 come from the fact that each X^- propagator is always sandwiched by two vertex couplings μ_1. Similarly, $B^*_{X^-}$ is a polynomial function of $\left(e^{i\xi_2}\right)^2$ and $\left(e^{i\xi_2}\right)^4$, where

$$\delta_1 - \phi_1 = \delta_2 - \phi_2 = \xi_2$$

Note that $Im(A_{tree}B^*_{X^-})$ is negligible in comparison to $Re[A_{tree}B^*_{X^-}]$. Therefore, the imaginary part of $\left(e^{i\xi}\right)^2$ can be neglected for the magnitude calculation, which makes

$$\begin{aligned} Re[e^{2i\xi_{1,2}}] &= \cos(2\xi_{1,2}), \\ Re[e^{4i\xi_{1,2}}] &= \cos(4\xi_{1,2}). \end{aligned} \tag{4.8}$$

Therefore we can write the asymmetry as

$$A_{\pm} = C_1[\cos(2\xi_1) - \cos(2\xi_2)] + C_2[\cos(4\xi_1) - \cos(4\xi_2)]. \tag{4.9}$$

Now $A_{\pm}$ have the maximum asymmetry magnitude (minimum) at $\delta_{1,2} = -\frac{3}{4}\pi + n\frac{1}{2}\pi$ and $\phi_{1,2} = \frac{3}{4}\pi + n\frac{1}{2}\pi$, where n=1, 2, 3, ...

4.5.1 Mass of $X^{\pm}$

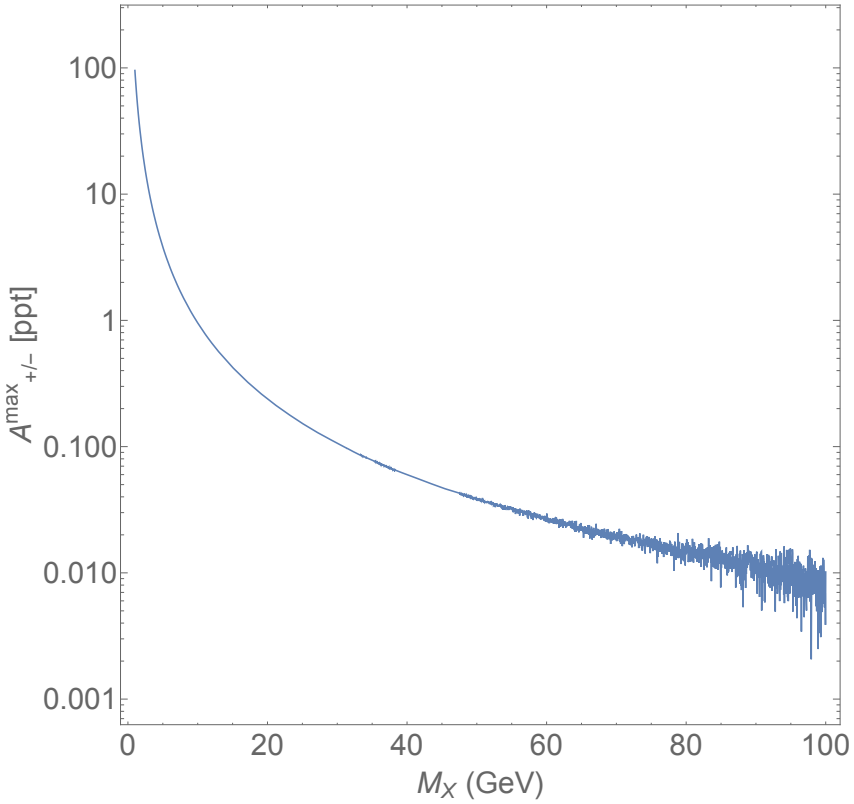

Figure 4.12: A_{max} in parts per trillion (ppt) vs Mass with $a_1 = 0.1, a_2 = 0.2$.

The values for a_1 and a_2 are picked only as an arbitrary reference. Note that the value of the asymmetry is small in this plot; however, it also depends on the coupling constants significantly.

Figure 4.12 shows the dependency between A_{max} and the mass of $X^{\pm}$. In general, A_{max} decreases when the mass increases nearly linearly. Comparing to effect of the coupling constants, the mass contribution to A_{max} is limited.

Unfortunately, it is not possible to explore the potential range for the mass of $X^{\pm}$ with the current LoopTools package. Since LoopTools is designed for the SM calculation, when the mass of the $X^{\pm}$ is above 80 GeV, it starts to rapidly lose numerical stability. Therefore, the default mass for further plots is at 50 GeV, where LoopTools still remains stable.

4.5.2 Coupling Constants

Since there is no phase factor involved in A_{max}, the coupling $\mu_{1,2} = a_1^2 + a_2^2$, which leaves A_{max} depends on a_1 and a_2 equally. For example, the plots in Figure 4.13 and Figure 4.14 below are identical.

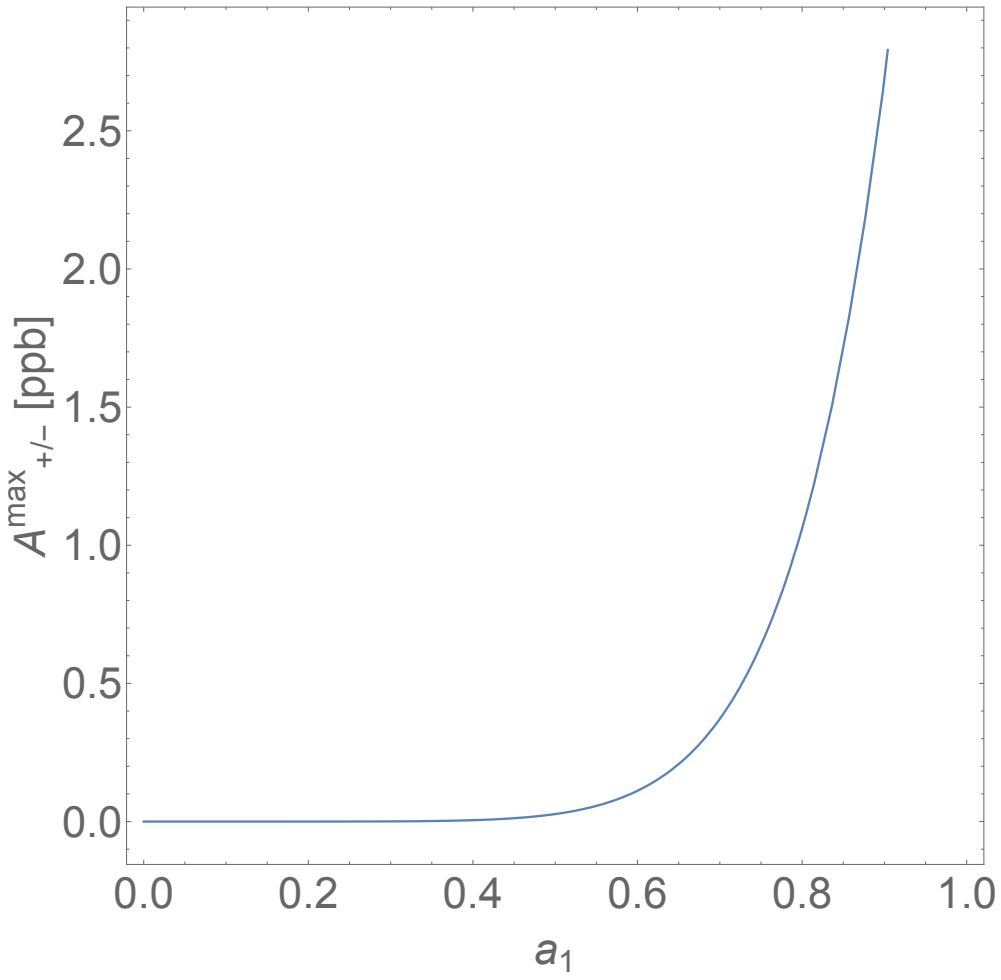

Figure 4.13: A_{max} in parts per billion (ppb) vs a_1, with $a_2 = 0.1$ and $m_X = 50$ GeV.

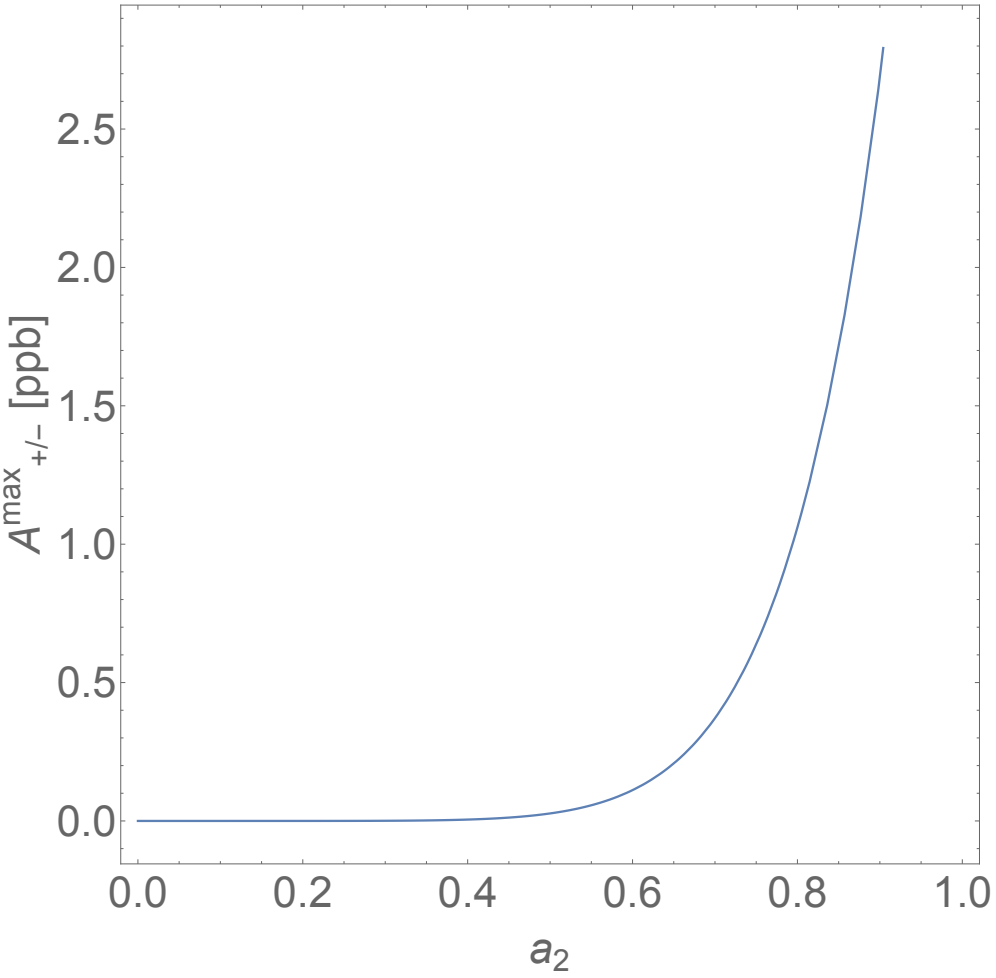

Figure 4.14: A_{max} in parts per billion (ppb) vs a_2, with $a_1 = 0.1$ and $m_X = 50$ GeV.

In general, A_{max} is an 8th order polynomial in $a_{1,2}$, which has a more significant impact on A_{max} than M_X does. The 8th order polynomial comes from $|\mathscr{M}|^2$, which contains terms of $\mu^4_{1,2}$ or $a^8_{1,2}$.

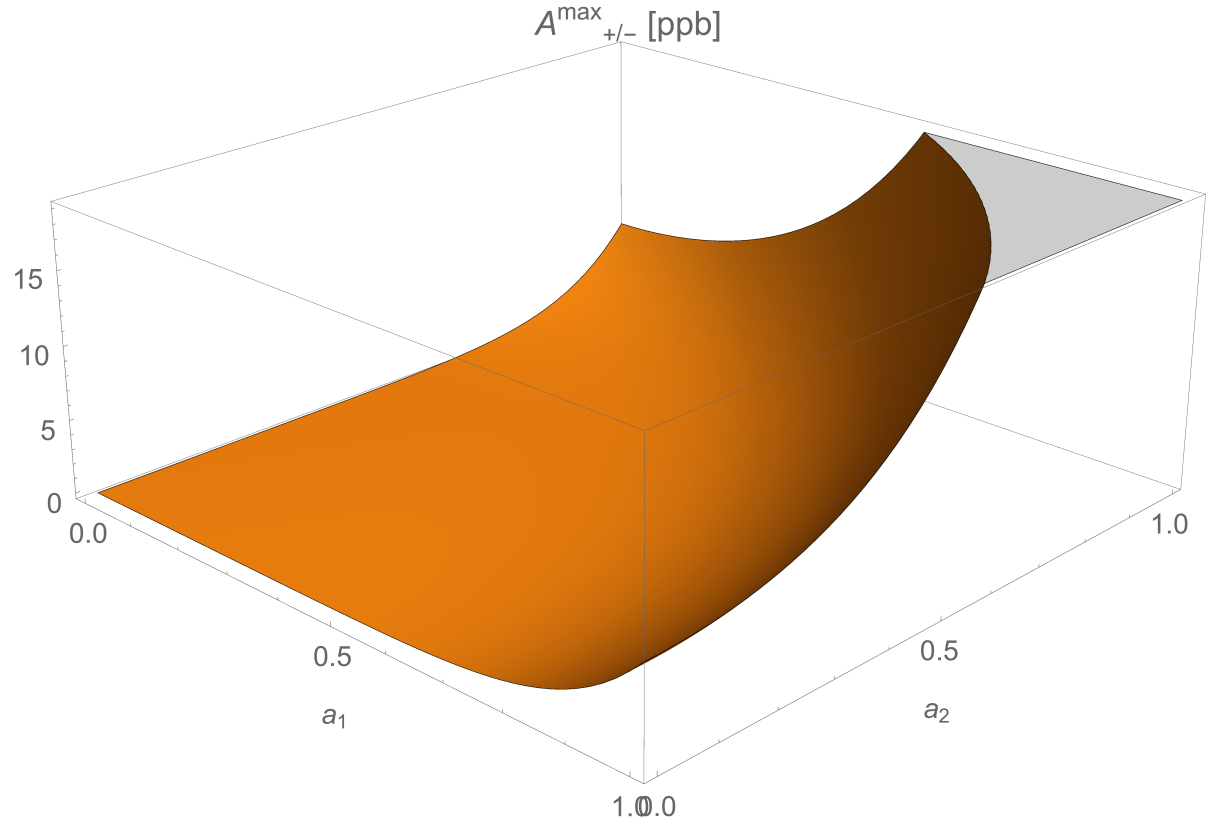

Figure 4.15: A_{max} in parts per billion (ppb) vs a_1 and a_2 with $m_X = 50$ GeV.

Thanks to $a_{1,2}$, the asymmetry can potentially have a sufficient magnitude to be measured. To do so, both cross sections of two scattering channels need to be measured. For Möller scattering, the high precision Möller scattering experiment at Thomas Jefferson National Accelerator Facility is at 2.4% overall accuracy in cross section asymmetry [5]. On the other hand, for positron-positron scattering, there is no precision experiment whatsoever. Additionally, the positron-positron scattering potentially poses more technical difficulty than Möller scattering due to its antimatter nature. One can expect the maximum accuracy to be less than 2.4%. Therefore, there is no complete physical measurement of asymmetry at the moment.

The main constraint of the parameters used in the calculation is the "naturalness" of the model. In effective theory, there is an convention that no scalar parameters should differ far from 1. Naturalness is not a mathematical requirement for any theory.

However, most of the coupling constants in SM do not differ greatly from 1.

Chapter 5

Conclusion

5.1 Mathematica

The Mathematica platform provids an excellent tool to run theoretical calculations for new physics models. There are well developed packages on Mathematica, such as FeynArts, Form, FormCalc and Looptools, for all the SM calculations. Since all the new physics particles are mixed or coupled with SM partners, the topology of the Feynman diagrams can be programmed in a similar way as the SM. It provides a lot of options and optimization, for one could specifically define all the couplings, propagators, renormalization scheme in an organized, algorithmic way.

Generally, the main difficulty is to implement the proper renormalization scheme, this is because it is quite complex in addition to the fact that not all fields are renormalizable. The stability of Looptools is also limited by the applied renormalization scheme. With the optimal scheme, Looptool loses its stability and generates unreliable results, such as shown in Figure 4.12.

5.2 $X^{\pm}$ Model

In chapter 3, many plots are shown to explore the influence of the $X^{\pm}$ model on the magnitude and phases of the asymmetry.

For the magnitude of cross section, there is no upper limit on the theoretical calculations thanks to the coupling constants. However, the coupling constants $a_{1,2}$ are not expected to be higher than 1 by the naturalness. The mass dependency for the asymmetry calculation was not stable above 80 GeV. The decreasing trend between the asymmetry magnitude and mass is clear. Due to the mass being involved in the denominator of propagators in the amplitude integrals, such a decreasing trend is expected.

The phase factors performed as designed. They introduce the asymmetry directly by assigning different phases for coupling a_1 and a_2. Such differences result in different cross sections. It is essential to include different phases for these two coupling. Otherwise the cross sections would be exactly the same. The four phase factors are physical constants, which need to be measured experimentally. The study of the phase factor pattern proves the mathematical reliability of the model.

5.3 Future Directions

There is more work needed to be done to use the $X^{\pm}$ model to fully explain strong CP violation. The main requirements are including the hadronic channels with the new model and the decay rate of $X^{\pm}$ into the electron, positron, and hadronic products. The hadronic channels can pose many potential problems due to their complexity. Despite the difficulty, it is essential to include them to complete the big picture for strong CP violation. There will be an updated model for $X^{\pm}$ including the coupling and renormalization scheme with the hadronic channels.

The next step is to connect strong CP violation with the dark matter and matter

asymmetric distribution, including additional dark matter particles in the model as the annihilation product of the $X^{\pm}$ particles. As a result, the $X^{\pm}$ model can propose a symmetry between matter-antimatter and dark matter-anti dark matter.

Appendices

Appendix A

Mathematica

```
SetDirectory["/Users/shihaowu/Research/FeynArts-3.9/"]
<< FeynArts`
<< /Users/shihaowu/Research/FormCalc-8.4/FormCalc_SQ-XM.m

CKM = IndexDelta;

Neglect[ME] = 0;
Neglect[ME2] = 0;

t1tree := CreateTopologies[0, 2 → 2]
t1brems := CreateTopologies[0, 2 → 3]
trtop := CreateTopologies[1, 1 → 2, ExcludeTopologies → {WFCorrections, Tadpoles}]
t1SE := CreateTopologies[1, 2 → 2,
  ExcludeTopologies → {WFCorrections, Tadpoles, AllBoxes, Triangles}]
t1TR := CreateTopologies[1, 2 → 2, ExcludeTopologies →
    {WFCorrections, Tadpoles, AllBoxes, SelfEnergies}]
t1Box := CreateTopologies[1, 2 → 2, ExcludeTopologies →
    {WFCorrections, Tadpoles, SelfEnergies, Triangles}]
t1SECT := CreateCTTopologies[1, 2 → 2, ExcludeTopologies →
    {WFCorrectionCTs, TadpoleCTs, AllBoxCTs, TriangleCTs}]
t1TRCT := CreateCTTopologies[1, 2 → 2, ExcludeTopologies →
    {WFCorrectionCTs, TadpoleCTs, AllBoxCTs, SelfEnergyCTs}]

t2TRtest :=
 InsertFields[trtop, {F[2, {1}]} → {F[2, {1}], V[1]}, InsertionLevel → {Particles},
  LastSelections → {! S, ! U}, Model → "X+-SM-NM", GenericModel → "X+-Lorentz-NM"]
t2treeG := InsertFields[t1tree, {F[2, {1}], F[2, {1}]} → {F[2, {1}], F[2, {1}]},
  InsertionLevel → {Particles}, ExcludeParticles → {V[2], S, U, DV[1], DV[2]},
  Model → "X+-SM-NM", GenericModel → "X+-Lorentz-NM"]
t2treeZ := InsertFields[t1tree, {F[2, {1}], F[2, {1}]} → {F[2, {1}], F[2, {1}]},
  InsertionLevel → {Particles}, ExcludeParticles → {V[1], S, U, DV[2]},
  Model → "X+-SM-NM", GenericModel → "X+-Lorentz-NM"]
t2TR1 := InsertFields[t1TR, {F[2, {1}], F[2, {1}]} → {F[2, {1}], F[2, {1}]},
  InsertionLevel → {Particles}, ExcludeFieldPoints → {},
  ExcludeParticles → {S[1], S[2], S[3], S[5], DV, V[3], X[2]},
  Model → "X+-SM-NM", GenericModel → "X+-Lorentz-NM"]
t2TR := DiagramDelete[t2TR1, {4 ...  7, 14 ...  17, 24 ...  27, 34 ...  37}]
t2Box0 := InsertFields[t1Box, {F[2, {1}], F[2, {1}]} → {F[2, {1}], F[2, {1}]},
  InsertionLevel → {Particles}, ExcludeParticles → {S[1], S[2], DV[2], V, S[3], S[5], X[2]},
  Model → "X+-SM-NM", GenericModel → "X+-Lorentz-NM"]
t2Box1 := t2Box0;
t2SECT1 := InsertFields[t1SECT,
  {F[2, {1}], F[2, {1}]} → {F[2, {1}], F[2, {1}]}, InsertionLevel → {Particles},
  ExcludeFieldPoints → {}, ExcludeParticles → {S[1], S[2], DV[2]},
  Model → "X+-SM-NM", GenericModel → "X+-Lorentz-NM"]
t2SECT := DiagramDelete[t2SECT1, {1, 2, 4, 6, 10, 11, 13, 15}]
t2TRCT := InsertFields[t1TRCT,
  {F[2, {1}], F[2, {1}]} → {F[2, {1}], F[2, {1}]}, InsertionLevel → {Particles},
  ExcludeFieldPoints → {}, ExcludeParticles → {S[1], S[2], DV[2]},
  Model → "X+-SM-NM", GenericModel → "X+-Lorentz-NM"]

Finite = 1;
MG0 = MZ;
MGp = MW;

SetOptions[InsertFields, InsertionLevel → {Particles},
 GenericModel → "X+-Lorentz-NM", Model → "X+-SM-NM"]
SetOptions[CalcFeynAmp, Dimension → D, FermionChains → Chiral,
 SortDen → True, FermionOrder → Automatic]
```

```
ampBox1 = CreateFeynAmp[t2Box1];
ampgtree = CreateFeynAmp[t2treeG];
ampTr = CreateFeynAmp[t2TR];
ampTrCT = CreateFeynAmp[t2TRCT];

stuffg = CalcFeynAmp[ampgtree];
stuffBox1 = CalcFeynAmp[ampBox1];
stuffTr = CalcFeynAmp[ampTr, ampTrCT];
stuffTrCT = CalcFeynAmp[ampTrCT];

MogTree =
  SquaredME[stuffg, stuffg] //. HelicityME[stuffg, stuffg] //. Subexpr[] //. Abbr[] //.
   k[n_] → kn[n];
MogBox = SquaredME[stuffg, stuffBox1] //. HelicityME[stuffg, stuffBox1] //. Subexpr[] //.
    Abbr[] //. k[n_] → kn[n];
MogTr = SquaredME[stuffg, stuffTr] //. HelicityME[stuffg, stuffTr] //. Subexpr[] //.
    Abbr[] //. k[n_] → kn[n];
MogAsym = (2 * MogBox + 2 * MogTr) / MogTree / 2;

renConst = CalcRenConst[stuffTr] //. Pair[k[3], k[3]] → ϵ;

Den[x_, y_] := 1/(x - y)

Install["/Users/shihaowu/Research/LoopTools-2.12/build/LoopTools"]

<< /Users/shihaowu/Research/Tools/kin2to2.m

pol[a_, b_] := Vec[ep[a][b]]

kn[n_] := Vec[k[n]]
s[n_] := Vec[ep[n][0]]

Mass[1] := ME
Mass[2] := ME
Mass[3] := ME
Mass[4] := ME
Mass2[1] := ME2
Mass2[2] := ME2
Mass2[3] := ME2
Mass2[4] := ME2

Charge[1] := 1
Charge[2] := 1
Charge[3] := 1
Charge[4] := 1
```

```
CW := Sqrt[CW2]
CW2 := MW2 / MZ2
SW := Sqrt[SW2]
SW2 := 1 - (MW2 / MZ2)
```

$$\text{p2in} := \frac{\left(\text{ecms}^2 + \text{Mass2}[2] - \text{Mass2}[1]\right)^2}{4 * \text{ecms}^2} - \text{Mass2}[2]$$

$$\text{p2out} := \frac{\left(\text{ecms}^2 + \text{Mass2}[4] - \text{Mass2}[3]\right)^2}{4 * \text{ecms}^2} - \text{Mass2}[4]$$

```
pin := Sqrt[p2in]
pout := Sqrt[p2out]
ef1 := Sqrt[p2in + Mass2[1]]
ef2 := Sqrt[p2in + Mass2[2]]
ef3 := Sqrt[p2out + Mass2[3]]
ef4 := Sqrt[p2out + Mass2[4]]
S := 2 * p2in + Mass2[1] + Mass2[2] + 2 * ef1 * ef2
T := Mass2[1] + Mass2[3] - 2 * (ef1 * ef3 - Sqrt[p2in * p2out] * Cos[theta])
U := Mass2[1] + Mass2[4] - 2 * (ef1 * ef4 + Sqrt[p2in * p2out] * Cos[theta])

Hel[1] = 0;
Hel[2] = 0;
Hel[3] = 0;
Hel[4] = 0;

MN := 0.939565379
MN2 := MN^2
ME := 0.510998928 * 10^-3
MU := 0.06983
MD := 0.06984
(*MU & MD changed from new mass file*)
MM := 105.6583715 * 10^-3
ML := 1776.82 * 10^-3
MC := 1.275
MB := 4.18
MT := 173.5
MS := 0.125
```

$$\text{Alfa} := \frac{1}{137.0359895}$$

```
Alfa2 := Alfa^2
MZ := 91.1876
MW := 80.385
MH := 125.0
MH2 := MH * MH
MM2 := MM * MM
ML2 := ML * ML
MC2 := MC * MC
MB2 := MB * MB
MT2 := MT * MT
MS2 := MS * MS
MZ2 := MZ * MZ
MW2 := MW * MW
MD2 := MD * MD
MU2 := MU * MU
ME2 := ME * ME

EL := 2 * Sqrt[Pi * Alfa]
Simplify[(S + T + U)] //. ecms → 20 //. theta → 40
```

```
2 * (ME2 + ME2)
```

```
SetLambda[10^0] (*IR*)
SetMudim[10^0] (*UV*)
SetDelta[0] (*UV*)
Elab := 11.0

dE := 5 * 10^-2 * Sqrt[S]
ecms := Sqrt[2 * Elab * ME]
theta := th * Pi/180

scV1 = 1;
scV2 = 1;
scV3 = 1;

δ1 = a;
ϕ1 = b;
δ2 = c;
ϕ2 = d;

Expand[
 MogAsym //. Subexpr[] //. Abbr[] //. renConst //. th → 90 //. epsc1 → 0.1 //. epsc2 → 0.2 //.
        PHAS1 → Exp[I * δ1 + I * ϕ1] //. PHAS2 → Exp[I * δ2 + I * ϕ2] //. PHAS3 → Exp[
        I * δ1 - I * ϕ1] //. PHAS4 → Exp[I * δ2 - I * ϕ2] //. MXP → 20 //. MXM → 20 //. ϵ → 0.0001]
```

Bibliography

[1] Victor Mukhamedovich Abazov, B Abbott, Bannanje Sripath Acharya, M Adams, Todd Adams, Guennadi D Alexeev, G Alkhazov, A Alton, G Alverson, GA Alves, et al. Search for w′→ tb resonances with left-and right-handed couplings to fermions. *Physics Letters B*, 699(3):145–150, 2011.

[2] F. Abe, H. Akimoto, A. Akopian, M. G. Albrow, S. R. Amendolia, D. Amidei, J. Antos, C. Anway-Wiese, S. Aota, G. Apollinari, and et al. Observation of Top Quark Production in pbar-p Collisions with the Collider Detector at Fermilab. *Physical Review Letters*, 74:2626–2631, April 1995. doi: 10.1103/PhysRevLett.74.2626.

[3] E Kh Akhmedov, GC Branco, and MN Rebelo. Seesaw mechanism and structure of neutrino mass matrix. *Physics Letters B*, 478(1):215–223, 2000.

[4] Riccardo Barbieri, Paolo Lodone, and David M Straub. Cp violation in supersymmetry with effective minimal flavour violation. *Journal of High Energy Physics*, 2011(5):1–21, 2011.

[5] J Benesch, P Brindza, RD Carlini, JP Chen, E Chudakov, S Covrig, MM Dalton, A Deur, D Gaskell, A Gavalya, et al. The moller experiment: An ultra-precise measurement of the weak mixing angle using möller scattering. *arXiv preprint arXiv:1411.4088*, 2014.

[6] M Benhamou and G Mahoux. Multiplicative renormalization of continuous polymer

theories, in good and θ solvents, up to critical dimensions. *Journal de Physique*, 47 (4):559–568, 1986.

[7] Laurie M. Brown. The idea of the neutrino. *Phys. Today*, Volume 31, September 1978.

[8] Gerhard Buchalla. Cp violation in k and b decays. *arXiv preprint hep-ph/9707545*, 1997.

[9] N. Cabibbo. Unitary Symmetry and Leptonic Decays. *Physical Review Letters*, 10: 531–533, June 1963. doi: 10.1103/PhysRevLett.10.531.

[10] J. H. Christenson, J. W. Cronin, V. L. Fitch, and R. Turlay. Evidence for the 2π decay of the k_2^0 meson. *Phys. Rev. Lett.*, 13:138–140, Jul 1964. doi: 10.1103/PhysRevLett.13.138. URL `http://link.aps.org/doi/10.1103/PhysRevLett.13.138`.

[11] G. D. Coughlan. *The ideas of particle physics : an introduction for scientists*. Cambridge University Press, Cambridge New York, 2006. ISBN 9780521677752.

[12] C. L. Cowan, Jr., F. Reines, F. B. Harrison, H. W. Kruse, and A. D. McGuire. Detection of the Free Neutrino: A Confirmation. *Science*, 124:103–104, July 1956. doi: 10.1126/science.124.3212.103.

[13] Richard H Cyburt. Primordial nucleosynthesis for the new cosmology: determining uncertainties and examining concordance. *Physical Review D*, 70(2):023505, 2004.

[14] Ansgar Denner and S Dittmaier. Reduction schemes for one-loop tensor integrals. *Nuclear Physics B*, 734(1):62–115, 2006.

[15] L. D. Faddeev and V. N. Popov. Feynman diagrams for the Yang-Mills field. *Physics Letters B*, 25:29–30, July 1967. doi: 10.1016/0370-2693(67)90067-6.

[16] Kazuo Fujikawa. Path integral for gauge theories with fermions. *Physical Review D*, 21(10):2848, 1980.

[17] Alberto Garfagnini. Neutrinoless double beta decay experiments. In *International Journal of Modern Physics: Conference Series*, volume 31, page 1460286. World Scientific, 2014.

[18] David Griffiths. *Introduction to elementary particles*. Wiley-VCH, Weinheim Germany, 2008. ISBN 9783527406012.

[19] G Grunberg. Renormalization-scheme-invariant qcd and qed: The method of effective charges. *Physical Review D*, 29(10):2315, 1984.

[20] Thomas Hahn. Feynman diagram calculations with feynarts, formcalc, and looptools. 2010.

[21] Tom Hartsfield. The standard model part i: The periodic table of physics, March 2012. URL `http://www.realclearscience.com/blog/2012/03/the-standard-model-part-i.html`.

[22] Xiao-Gang He and Lu-Hsing Tsai. Spontaneous cp violating phase as the phase in pmns matrix. *The European Physical Journal C*, 71(3):1–8, 2011.

[23] Tarek Ibrahim and Pran Nath. Phases and cp violation in susy. *arXiv preprint hep-ph/0210251*, 2002.

[24] Sabine Kraml. Cp violation in susy. *arXiv preprint arXiv:0710.5117*, 2007.

[25] Manfred Lindner, Tommy Ohlsson, and Gerhart Seidl. Seesaw mechanisms for dirac and majorana neutrino masses. *Physical Review D*, 65(5):053014, 2002.

[26] Markus A Luty. Baryogenesis via leptogenesis. *Physical Review D*, 45(2):455, 1992.

[27] Ernest Ma. Verifiable radiative seesaw mechanism of neutrino mass and dark matter. *Physical Review D*, 73(7):077301, 2006.

[28] Z. Maki, M. Nakagawa, and S. Sakata. Remarks on the Unified Model of Elementary Particles. *Progress of Theoretical Physics*, 28:870–880, November 1962. doi: 10.1143/PTP.28.870.

[29] S. Mandelstam. Determination of the Pion-Nucleon Scattering Amplitude from Dispersion Relations and Unitarity. General Theory. *Physical Review*, 112: 1344–1360, November 1958. doi: 10.1103/PhysRev.112.1344.

[30] Palash B Pal. Dirac, majorana, and weyl fermions. *American Journal of Physics*, 79(5):485–498, 2011.

[31] Michael Peskin. *An introduction to quantum field theory*. Addison-Wesley, Reading, Mass, 1995. ISBN 978-0201503975.

[32] M Riazuddin. Particle aspects of cosmology and baryogenesis. 2003.

[33] Matthew Robinson. *Symmetry and the standard model mathematics and particle physics*. Springer, New York, 2011. ISBN 978-1-4419-8266-7.

[34] Antonella Del Rosso. Higgs: the beginning of the exploration. (BUL-NA-2012-357. 47/2012):3, Nov 2012.

[35] A. D. Sakharov. SPECIAL ISSUE: Violation of CP in variance, C asymmetry, and baryon asymmetry of the universe. *Soviet Physics Uspekhi*, 34:392–393, May 1991. doi: 10.1070/PU1991v034n05ABEH002497.

[36] Jos AM Vermaseren. New features of form. *arXiv preprint math-ph/0010025*, 2000.

[37] Wikipedia, the free encyclopedia. Standard model, 2013. URL `http://cdn.phys.org/newman/gfx/news/2015/particlephys.png`. [Online; accessed May 8, 2013].

[38] Wikipedia, the free encyclopedia. Standard model (mathematical formulation), 2015. URL `https://en.wikipedia.org/wiki/Standard_Model_(mathematical_`

formulation)#/media/File:
Standard_Model_Of_Particle_Physics--Most_Complete_Diagram.png. [Online; accessed March 29, 2016].